III.7 Safety Analyses

Preliminary analyses have been completed to assess the potential safety performance characteristics of the Advanced Burner Reactor (ABR) 1000 MW_{th} design. The scope of the analyses presented here focuses on the ability of ABR to provide inherent protection against damaging consequences in low probability accident sequences involving multiple equipment failures.

III.7.1 Background and Summary

A summary description of the accident sequences analyzed and the results obtained are first presented. Detailed descriptions of the analyses are provided in subsequent sections. In particular, Section III.7.2 contains a description of the analysis scope and initial reactor state, while Section III.7.3 describes the analysis methods modeling data and Section III.7.4 contains a more detailed account of the transient results.

III.7.1.1 Analysis Background

One of the primary goals in the ABR design is to provide not only the customary safety margins in design basis events, but also to deliver superior safety performance in beyond design basis events involving multiple equipment failures or unplanned operator actions. Consequently, the preliminary analyses presented here examine the behavior of the ABR in response to an accident initiator that is normally considered to have a low occurrence frequency but potentially severe consequences, especially when engineered safety systems are assumed to fail. The analyses consider the response of both metal-fueled and oxide-fueled cores to the transient conditions.

The accident initiator examined here is the total loss of normal power to the reactor cooling system while the plant is operating at full rated power. Within the plant, the effect of this initiator is the loss of normal operation of all reactor and feed-water coolant pumps. According to design, the plant responds with a reactor scram, with activation of emergency power supplies (diesel generators and batteries), and with activation of the normal shutdown heat removal mode. The normal shutdown heat removal path is through the reactor coolant system and steam generators, with auxiliary power supplied by the emergency power supplies. As a backup, a low-capacity emergency heat removal system is provided to remove heat directly from the reactor without the need for emergency power.

For the transient accident sequences analyzed here, the loss of power is accompanied by a complete failure of the emergency power supply system, resulting in a total loss of power to the reactor and intermediate coolant pumps. It is also assumed that the power generation plant immediately ceases operation, and provides no heat rejection capacity through the steam generators. The sole heat removal path following the loss of forced coolant flow is through the emergency heat removal system by natural circulation. This sequence was analyzed for the case with an immediate reactor scram and for the case without reactor scram. These cases are identified as the protected loss-of-flow (PLOF) and the unprotected loss-of-flow (ULOF) cases respectively. The PLOF and ULOF accident sequences both assume multiple equipment failures, failures of safety grade protection and cooling systems, and no operator actions. These sequences are an extreme

test of the ABR to provide inherent self-protection against the consequences of the most severe accident initiators.

III.7.1.2 Results Summary

The base cases for both the metal and oxide core designs are for the beginning of equilibrium cycle conditions. The detailed analysis results for the PLOF and ULOF accident sequences are presented in Section III.7.4, below. In addition to the base cases, parametric variations have also been performed for the ULOF accident sequence for both the metallic-fueled and the oxide-fueled cores. Parametric variations for the metal core involve changes to the control-rod driveline (CRDL) expansion reactivity feedback. Parametric variations for the oxide core also involve the CRDL reactivity feedback, but additional results are presented for the case where a self-actuated shutdown system (SASS) is employed. The SASS could be a secondary or a tertiary shutdown system. The specific SASS device selected for the analysis presented here is based on a safety rod passive de-latch mechanism utilizing magnetic resistance change at the Curie point temperature of the sensing alloy. Although these sequences simulate accidents that for some reactor designs may cause damage to the fuel and possibly progress into severe accident conditions, in the ABR these events cause no damage. During the accident sequences, reactor fuel, cladding, and coolant temperatures remain below safety limits.

In the PLOF sequence, the loss of forced coolant flow and normal heat removal is accompanied immediately by a reactor scram, which quickly brings the reactor power to decay heat levels. Early in the sequence, the emergency decay heat removal system does not have sufficient capacity to remove all the heat being produced, so system temperatures rise. However, due to the large heat capacity of the sodium-cooled pool-type concept, the ABR is able to absorb a significant amount of energy with only a slight temperature increase, and the natural circulation capability of the ABR promotes heat removal through the available emergency heat sink. After about six hours, the reactor decay heat falls to the capacity of the emergency heat removal system, and system temperatures begin to decrease. The analysis predicts that short coolant and cladding temperature spikes occur during the transition to natural circulation, but no fuel damage or cladding failures would occur. These conclusions hold for both the metal core and the oxide core, although some quantitative differences exist due to differences in core pressure drop (due to differences in the hydraulic resistances of the respective pin bundles) and differences in the initial stored energy (due to the higher operating temperature of oxide fuel).

In the ULOF accident, the reactor safety system fails to scram the reactor upon loss of forced coolant flow and normal heat removal, so the reactor remains at full power initially. Within the first minute, reactor temperatures increase as the coolant flow rate decreases, and inherent reactivity feedbacks reduce the reactor power. During this time, peak cladding temperatures rise to approximately 700°C for the metal core and 750°C for the oxide core. As coolant flow continues to decline, a second temperature peak occurs, and peak cladding temperatures reach approximately 550°C for the metal core and 800°C for the oxide core. This increase in temperature provides the necessary driving force to establish natural circulation flow. The development of natural circulation holds the slowly-rising peak cladding temperatures to around 800°C for the oxide core, but even

after six hours into the transient the fission power remains a significant part of the total power and the DRACS heat removal capability is still below the total heat production rate. The oxide system continues slowly heating up. The situation is quite different for the metal core where the peak fuel *and* cladding temperatures are reduced to about 520°C after six hours and the decay heat dominates. At this point the DRACS heat removal capability is reaching the total heat production rate, after which temperatures can be expected to remain stable. There is also a difference in the coolant boiling margin. The ULOF parametric feedback cases show a boiling margin of around 220°C to 250°C for the metal cases, but of only 50°C to 150°C for the oxide cases without the benefit of a SASS scram. The results also show that with the use of a SASS scram, the coolant boiling margin for the most challenging oxide case can be increased from 50°C to 170°C.

The primary significance of the analysis results is that both metal and oxide core designs demonstrate significant safety margins to coolant boiling and fuel damage in PLOF accident sequences. The metal core design also exhibits significant safety margins in the ULOF accident sequence. This is a direct consequence of the high thermal conductivity and low operating temperature of metal fuel, and the favorable negative feedback due to thermal expansion. However, the ULOF analyses for the oxide core design indicate that margins to coolant boiling will not be adequate without additional accident mitigation features. Inadequate margins exist for the oxide core design despite the use of a significantly longer flow halving time (20 seconds) compared to that used for the metal core (five seconds). The initially high oxide operating temperatures result in significant positive Doppler feedback when trying to reduce temperatures. Additional enhancements, such as a self-actuating shutdown (SASS) device will be required for the oxide core to increase safety margins so that no fuel damage or cladding failures would occur, even when multiple safety systems are assumed to malfunction. Nevertheless, the neutronic, thermal, and hydraulic performance characteristics of the ABR design provide a defensive barrier to reactor damage for accident initiators that otherwise progress into severe accident conditions. Such superior safety characteristics are inherent to a sodium-cooled, pool-type reactor concept.

III.7.2 Analysis Scope

The analysis results reported here were selected on the basis that they show the safety margins and the inherent ability of a sodium-cooled, pool-type reactor system to provide protection against severe, damaging consequences. The accident sequences analyzed are near the end of the spectrum of the most pessimistic, challenging, and potentially damaging events. The analysis results demonstrate the passive safety performance advantages of the ABR. This performance is possible because of the favorable natural circulation shutdown heat removal capability that is possible with low pressure sodium coolant in a pool configuration. In addition, metallic fuel provides significant inherent safety performance due to its superior heat transfer and reactivity feedback characteristics.

III.7.2.1 Accident Sequences

The basic accident sequence analyzed is the loss of normal power to the reactor and intermediate coolant pumps, with failure of the emergency power supplies. The result is a loss of forced flow in the primary and intermediate coolant circuits, although mechanical

pump inertia will provide for a coast-down in the coolant flow during the very early part of the transient. In addition, it is assumed that heat removal through the steam generator ceases, so that the only heat removal path is through the emergency direct reactor auxiliary cooling system (DRACS).

The natural circulation DRACS consists of heat exchangers located in the cold pool region within the reactor vessel, air dump heat exchangers located outside containment, and the connecting piping. The working fluid in the DRACS is NaK, and fluid flow is by natural circulation. Multiple independent DRACS units are provided for defense in depth. The DRACS is designed to remove 0.5% of full power (5000 kW) at normal operating temperatures assuming failure of one DRACS unit. The DRACS system operates continuously, with heat losses limited in normal operation by dampers on the NaK-to-air heat exchangers. In all the accident sequences analyzed here, one DRACS unit is assumed to fail, leaving a nominal system heat rejection capacity of 5000 kW.

The initial condition for the accident sequence is normal operation at full power and flow. With the loss of pumping power, flow in the primary circuit coasts down according to the spinning inertia of the pumps and motors. Following flow coast down, natural circulation flow is established.

With the loss of power, forced flow in the intermediate coolant system is also lost. Further, it is assumed that heat rejection through the steam generator ceases. The intermediate heat transport system (IHTS) is alternately a heat sink or source in the accident sequence, depending on its temperature and the primary system temperature at the intermediate heat exchanger (IHX). During the transient, natural circulation flow in the IHTS may reverse, depending on transient temperature conditions.

Two variations of the loss-of-flow accident sequence have been analyzed. In the first, it is assumed that the reactor safety system acts as designed to insert control rods and reduce reactor power immediately to decay heat. This sequence is called the protected loss-of-flow (PLOF) accident. In the second analysis, it is assumed that the reactor safety system fails to insert the scram control rods, and the loss of forced flow proceeds at full power. This sequence is called the unprotected loss-of-flow (ULOF).

In the PLOF sequence, the absence of normal shutdown heat removal through the reactor coolant system causes a slow system temperature rise following the reactor scram. This temperature increase occurs because the DRACS has insufficient heat removal capacity to overcome both the early decay heat production rate and the stored heat in the primary and intermediate systems. Eventually, the decay heat falls below the DRACS capacity, and the system temperature declines.

In the ULOF sequence, the system temperature rises significantly with the flow coast down, but the core temperature rise introduces negative reactivity that acts to reduce the reactor fission power. In general, negative reactivity feedback effects will cause the reactor to seek equilibrium with the available heat sink by reducing power, but there are important differences between the metal and oxide cores. For the metal core, the reduction in power has the effect of reducing the reactor temperature and establishing a quasi-equilibrium condition. However, until the decay heat falls below the available heat rejection capacity, the reactor system will continue to heat slowly, with the long term temperature rise buffered by the thermal heat inertia of the system. When decay heat

production falls below the DRACS capacity, the system temperature declines. For the oxide core, the positive Doppler feedback tends to limit the net reduction in power, thereby inhibiting the reduction in reactor temperatures.

III.7.2.2 Reactor State

Safety analyses were performed for the beginning-of-equilibrium-cycle (BOEC) reactor conditions described in Section II.1.1. For the BOEC safety analysis of the metal core, it was assumed that sufficient irradiation had taken place to swell the fuel radially into contact with the cladding. Examination of EBR-II irradiated fuel has indicated that fuel-cladding contact will occur early in fuel life (1% burnup), depending on the initial geometry and local specific power. Fuel-cladding contact has the impact of lowering thermal resistance by eliminating the sodium-filled fuel-cladding gap. For the oxide core, calculations were carried out to determine pre-accident conditions of the fuel, including radial expansion, central void formation, and fuel porosity and cracking.

In both the PLOF and ULOF analyses, the decay heat curve was taken as 100% of the ANSI 5.1 standard [1] for Pu-239. For the ULOF analysis, the decay heat curve was combined with the computed fission power calculated using the reactivity feedback parameters determined by the reactor physics analysis of Section II.1.1.

III.7.3 Analysis Methods and Input Data

The analytical methods used to evaluate the ABR performance are incorporated into the SAS4A/SASSYS-1 computer code [2] which was used to produce all the safety analysis results presented here. In the following sections, the reactor and coolant system thermal-hydraulic models are described along with key input data relevant to the determination of ABR safety performance.

III.7.3.1 Reactor Thermal Hydraulics

The thermal-hydraulic performance of the reactor core is analyzed with a geometric model consisting of a number of single-pin channels. In a multiple-channel, whole-core model, each channel represents a single fuel pin and its associated coolant and structure. The single pin is assumed to characterize the average pin in a fuel subassembly, and subassemblies with similar reactor physics and thermal-hydraulics characteristics are grouped, so a number of channels are selected to represent all the pins in the reactor core.

The geometry assumed in the channel thermal-hydraulic model is shown in Figure III.7-1. Heat generated in the fuel is assumed to travel through the cylindrically-symmetric pin to the upward-flowing coolant. The structure field is used to represent part of the hexagonal duct and the wire wrap. One-dimensional, radial heat transfer calculations are performed at many axial locations to model heat transfer from the fuel through the cladding to the coolant, and from the coolant to the structure, the gas plenum, and the reflectors. One-dimensional (axial) coolant mass flow is modeled with a momentum equation solution for the axial pressure profile, and convective heat transfer conditions are assumed at the interfaces between the coolant and the cladding, the reflectors, and the structure. Temperatures are calculated at multiple radial nodes in the fuel, the cladding, the reflectors, and the structure. A single bulk coolant temperature is calculated at each axial location. Axial heat conduction is neglected.

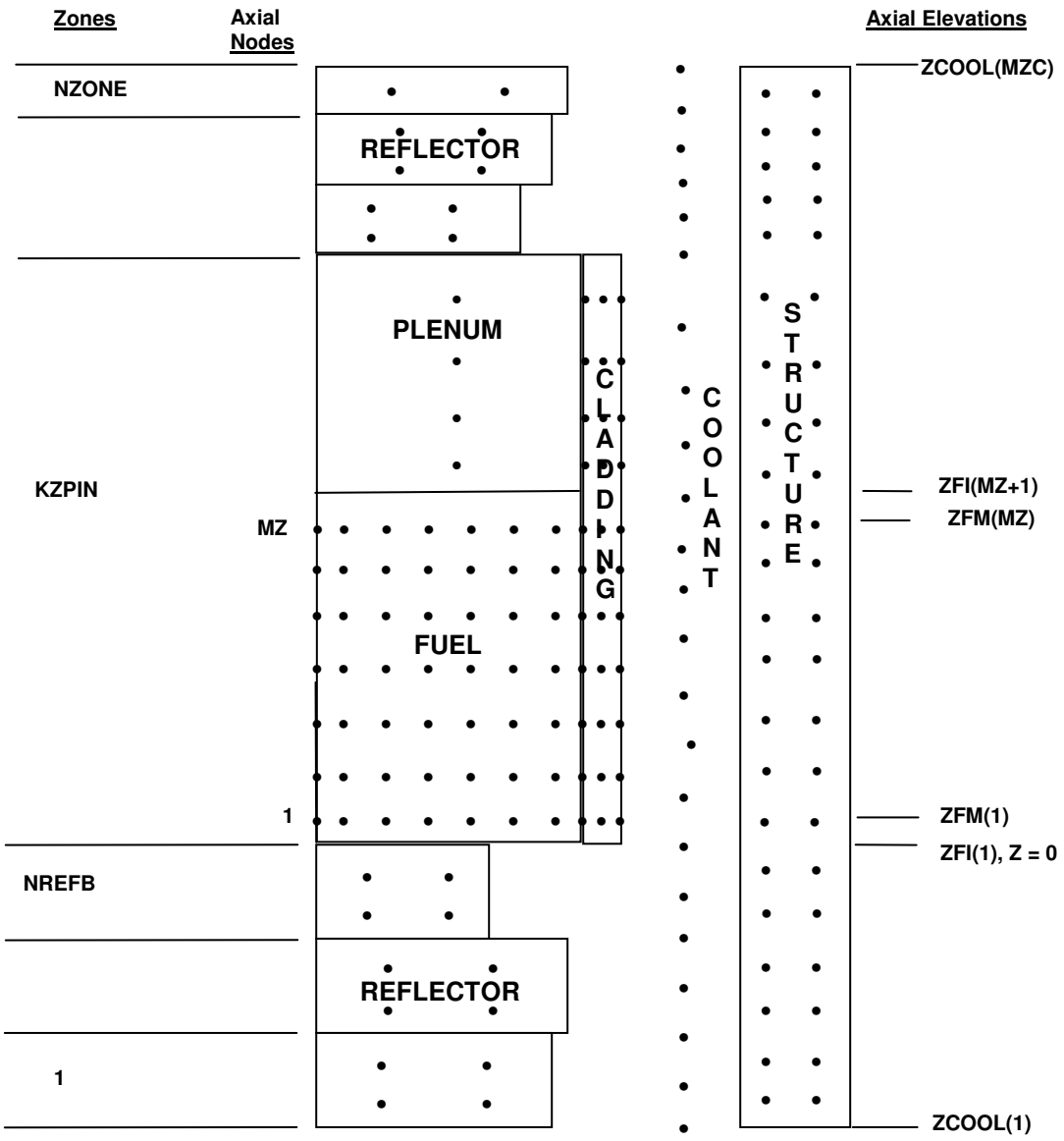

Figure III.7-1: SAS4A/SASSYS-1 Single-Pin Channel Model

Thermal, transport, and physical properties data for the coolant were taken as the temperature-dependent liquid sodium properties available in SAS4A/SASSYS-1. Cladding properties were taken as the HT9 data presented in Reference 3. Fuel properties for metal fuel were taken from the SSCOMP correlations in SAS4A/SASSYS-1 Version 3.0; these correlations are based on data generated in the Integral Fast Reactor (IFR) Program. Fuel properties for both pre-transient and transient behavior of oxide fuel are based on the DEFORM-4 module of SAS4A/SASSYS-1.

On the basis of the reactor physics calculations, the multiple-channel model depicted in Figure III.7-2 was selected for safety analysis calculations. This model approximates the full heterogeneity of the reactor physics model by assigning channels to represent each fuel enrichment zone. Channels 1 and 2 represent the average subassemblies in the inner and outer enrichment zones, respectively. Channel 3 represents all of the non-fuel subassemblies, including reflector and control assemblies. A fourth channel is used to represent the peak power-to-flow subassembly containing fresh fuel. The peak assembly is selected based on the highest power-to-coolant-flow ratio. For both metal and oxide cores, the peak power-to-flow assembly is one of the inner-core assemblies although the location of the peak assembly is different, as shown in Figure III.7-2.

Table III.7-I shows the geometric input data employed in the multiple-channel whole-core model. For the metal fuel, it has been assumed that the irradiated fuel has swollen into contact with the cladding. For the oxide fuel, the DEFORM-4 model in SAS4A/SASSYS-1 is used to calculate the radial swelling of the oxide fuel under steady-state radiation. The swelling is calculated for each axial node such that in some axial location the gap between the fuel and cladding could be closed while in other locations it could still be present. The thermal conductivity of the gap, initially filled with helium, is calculated by DEFORM-4 at each axial location.

The reflector channel power and flow rate represent average power and flow for all non-fuel assemblies in the core, including primary and secondary control rods and reflectors. The reflector channel is assumed to be represented by the reflector assembly geometry.

Axial power profiles in the core region are assumed to be identical for all assemblies. The power profile for the SAS4A/SASSYS-1 axial mesh, presented in Figure III.7-1, was calculated based on the five-region core power density for core assembly (IC34). The five-region power density was fitted with a fourth-degree polynomial in a way that the region-average values are conserved. Figure III.7-3 shows the five-region core average and peak power densities as well as the polynomial fit to the power profile for metal and oxide fuel cores.

Figure III.7-4 shows the initial subassembly powers for the BOEC condition. The subassembly power for the peak assembly assumes fresh fuel. All other subassembly powers represent channel averages from BOEC fuel compositions at various stages of depletion. Subassembly coolant flow rates at steady-state conditions are shown in Figure III.7-5. Coolant flow rates are from the flow-orifice calculations described in Section II.1.1.

Based on the above input conditions, SAS4A/SASSYS-1 calculates the initial, steady-state, thermal-hydraulic conditions in the reactor core prior to the onset of a transient. Peak coolant outlet, peak cladding, and peak fuel temperatures are shown in Figures III.7-6, III.7-7, and III.7-8, respectively. Coolant, cladding, and fuel temperatures that arise during a transient are discussed in the relevant sections below.

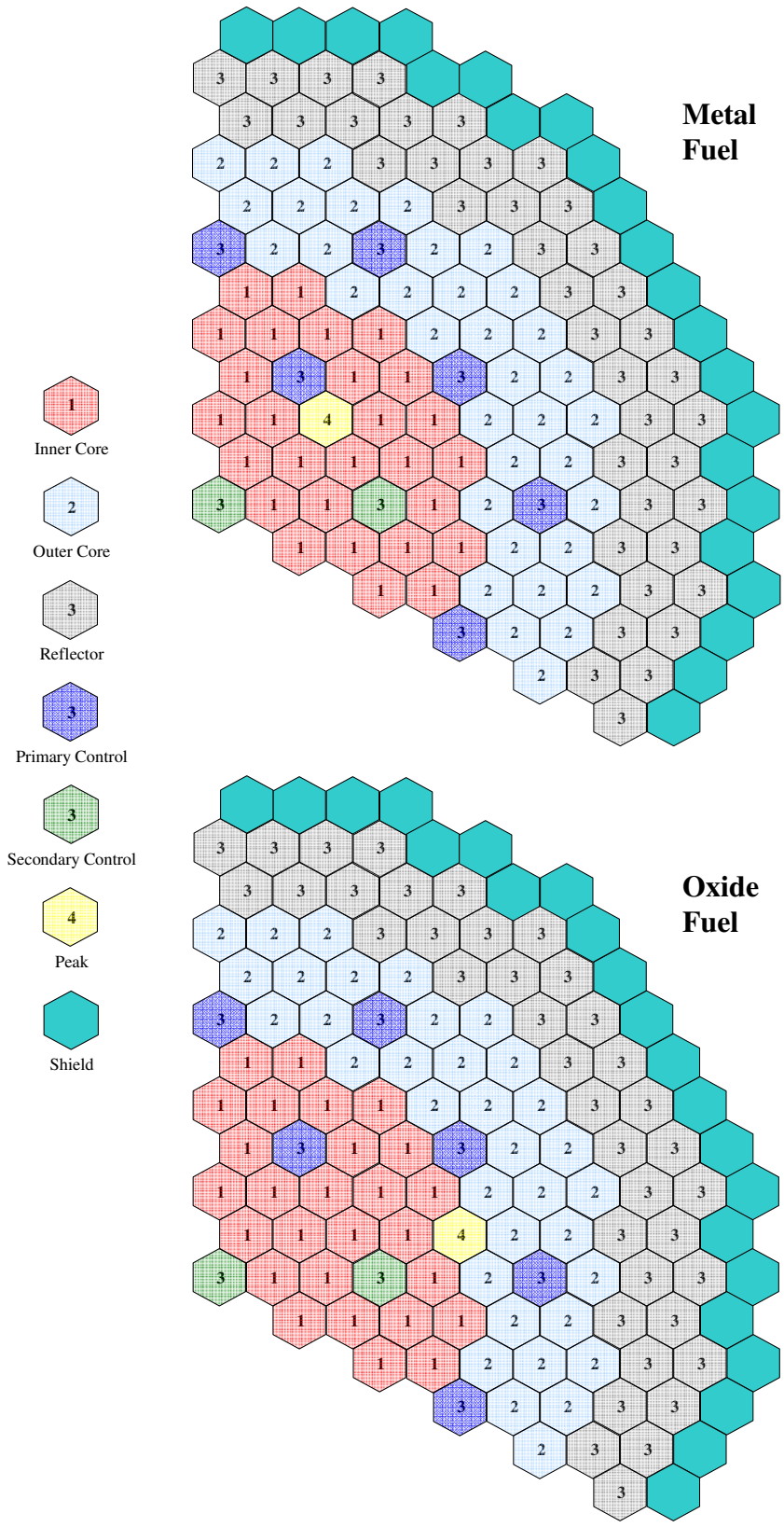

Figure III.7-2: Channel Assignment for Reactor Core Thermal-Hydraulic Model

Table III.7-I: Fuel Assembly, Pin, and Coolant Channel Model Data

	Metal Fuel	**Oxide Fuel**	**Reflector**
Pins per Assembly	271	271	91
Number of Assemblies	180	180	133
Channel 1 (Inner Core)	77	77	-
Channel 2 (Outer Core)	102	102	-
Channel 3 (Reflector)	-	-	133
Channel 4 (Peak)	1	1	-
Fuel Height, mm	812.8	1066.8	-
Gas Plenum Height, mm	1244.6	1600.2	-
Upper Reflector Height, mm	1117.6	635	-
Lower Reflector Height, mm	1244.6	1117.6	-
Axial Node Height, mm			
Core	40.6	53.3	same as fuel assembly
Gas Plenum	207.4	266.7	
Upper Reflector	223.5	127.0	
Lower Reflector	248.9	223.5	
Hydraulic Diameter, mm	3.361	3.361	1.878
Coolant Flow Area per Pin, mm^2	25.03	25.03	25.40
Outer Fuel Radius, mm	3.22	3.13	-
Inner Cladding Radius, mm	3.22	3.22	-
Outer Cladding Radius, mm	3.78	3.78	7.71
Structure Thickness [a], mm	4.50	4.50	4.50
Structure Perimeter [b] per Pin, mm	2.21	2.21	5.68
Reflector Thickness, mm	1.89	1.89	3.85
Reflector Perimeter, mm	23.72	23.72	48.41

a. Structure thickness includes weighted contribution from the inter-assembly gap sodium.
b. Structure perimeter includes contribution from wire wrap spacers.

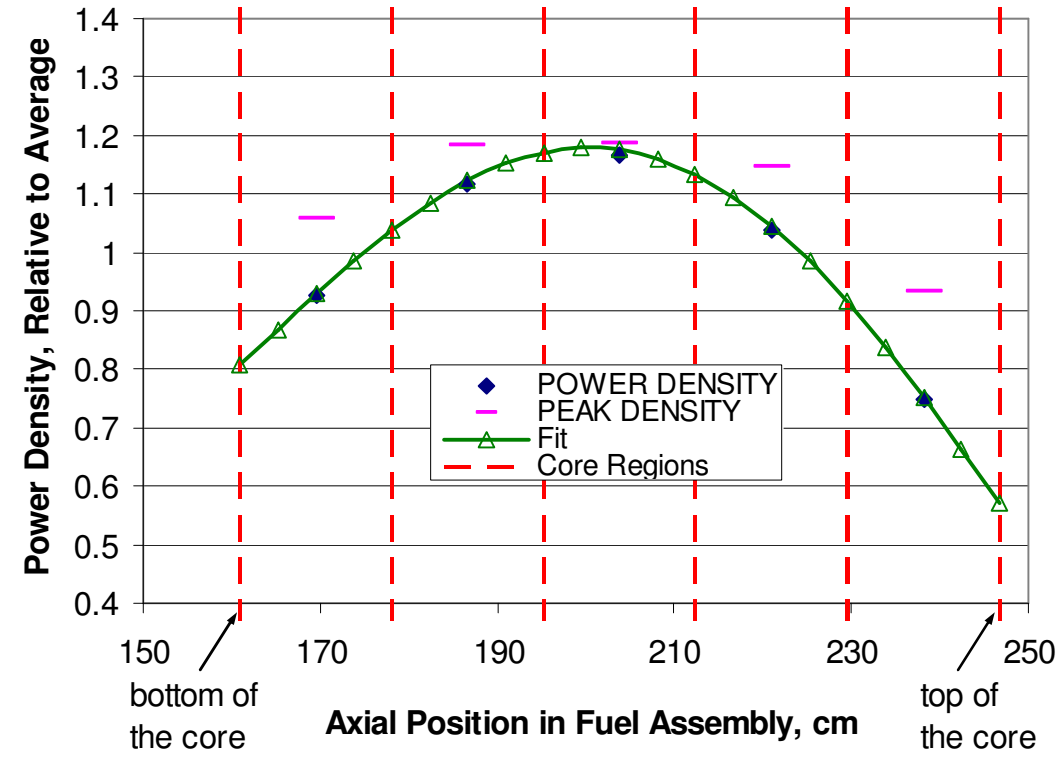

a) Metal Fuel Core

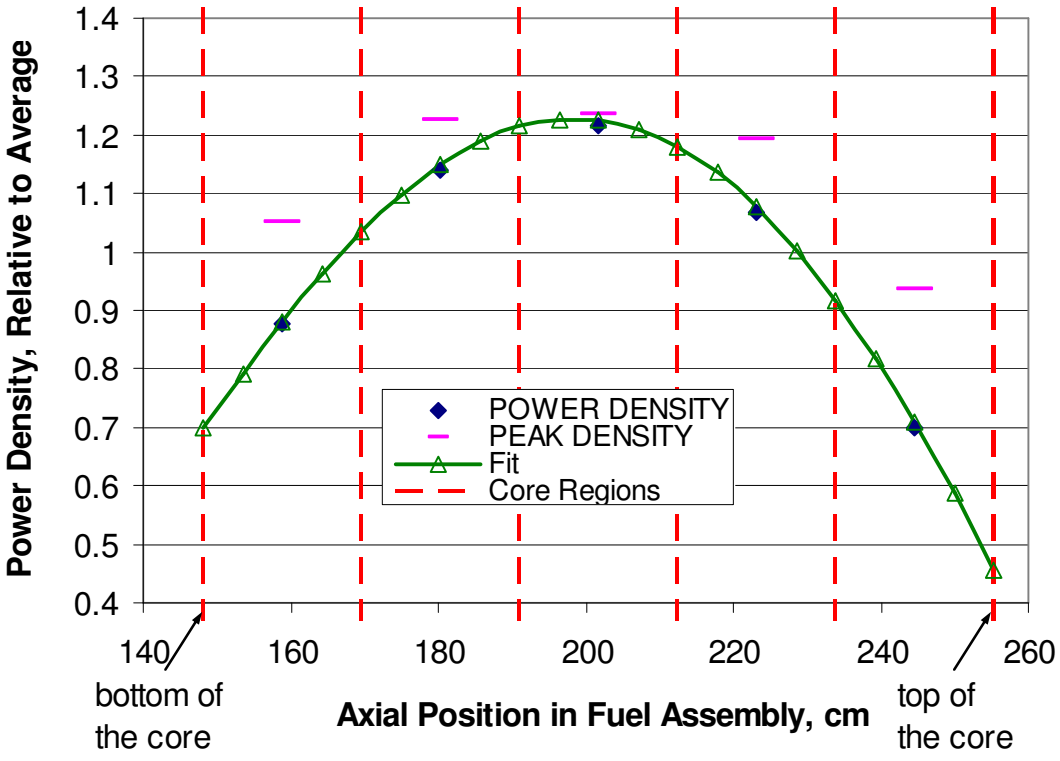

b) Oxide Fuel Core

Figure III.7-3: Core Power Profiles for SAS4A/SASSYS-1 Model.

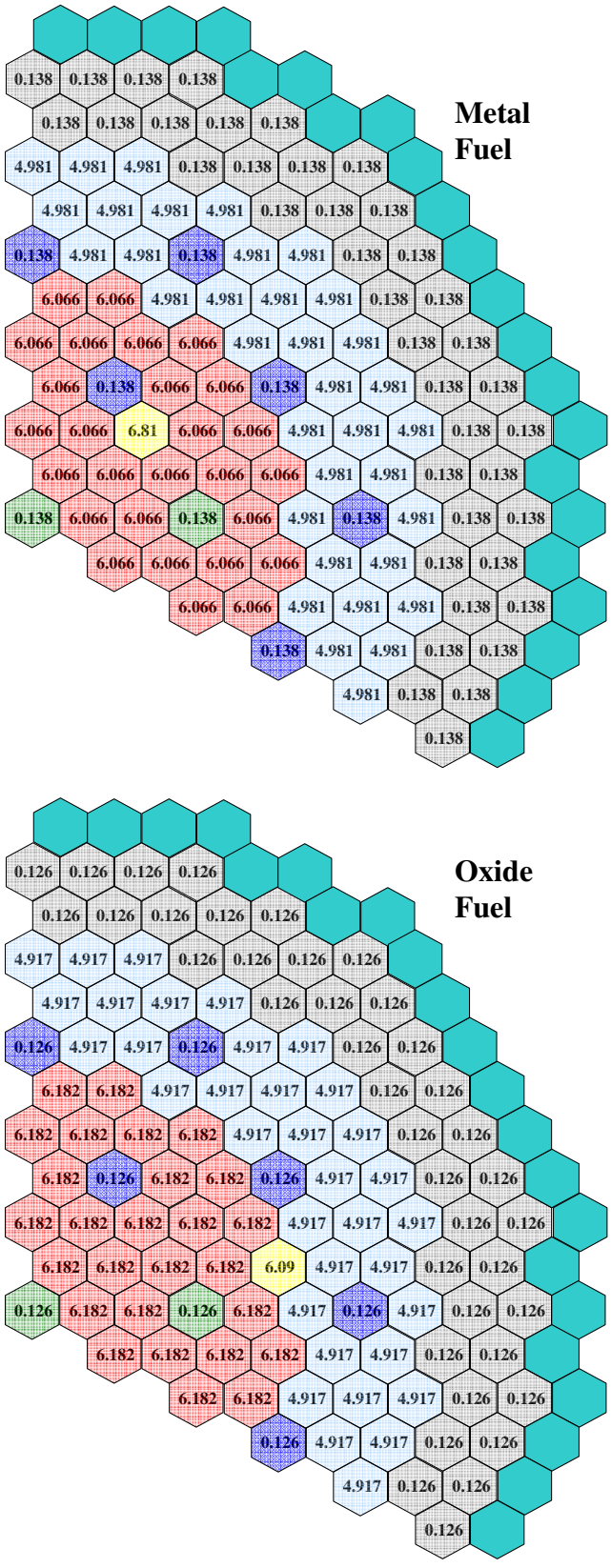

Figure III.7-4: BOEC Initial Subassembly Power (MW)

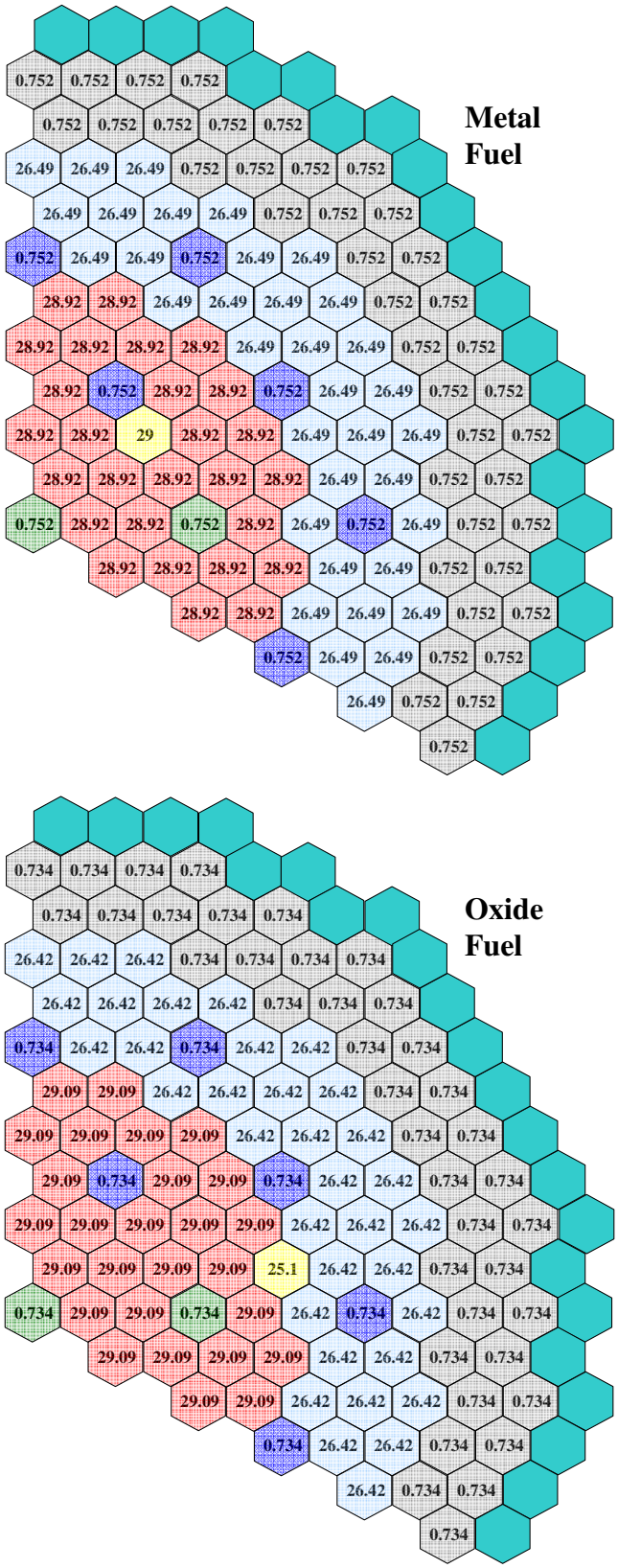

Figure III.7-5: Initial Subassembly Coolant Flow (kg/s)

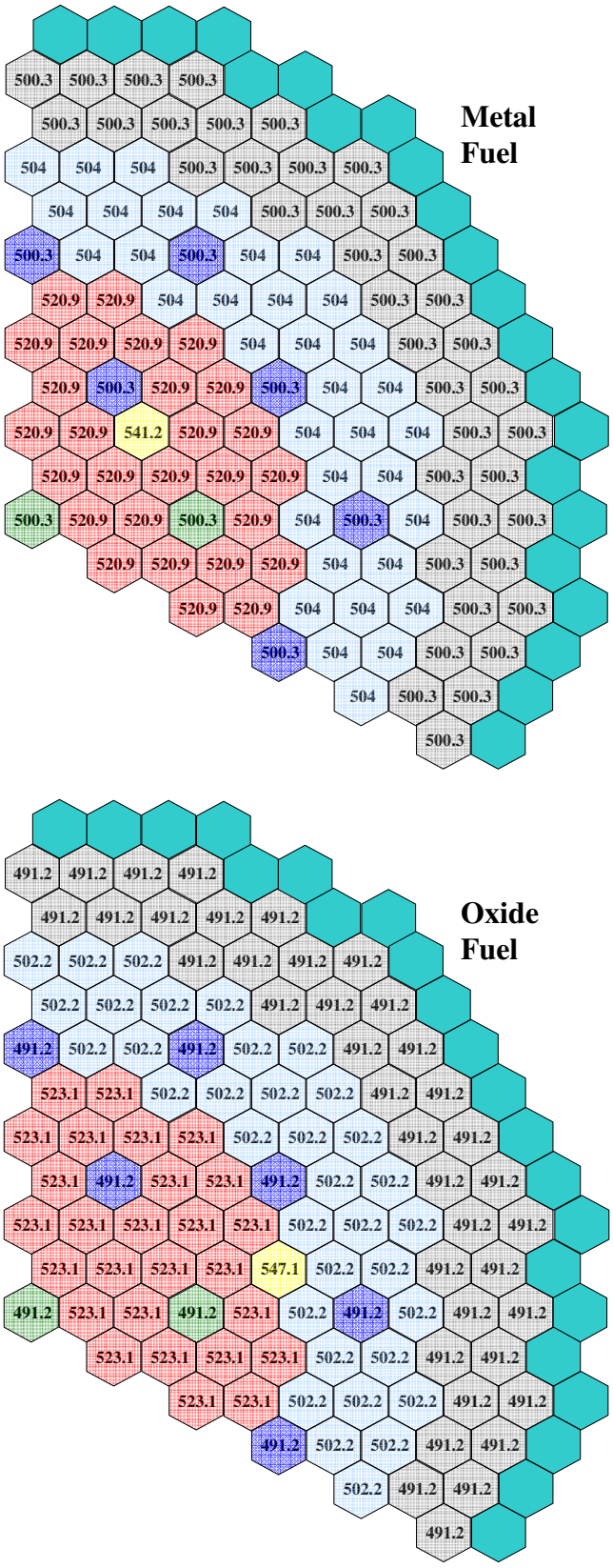

Figure III.7-6: BOEC Initial Coolant Outlet Temperature (°C)

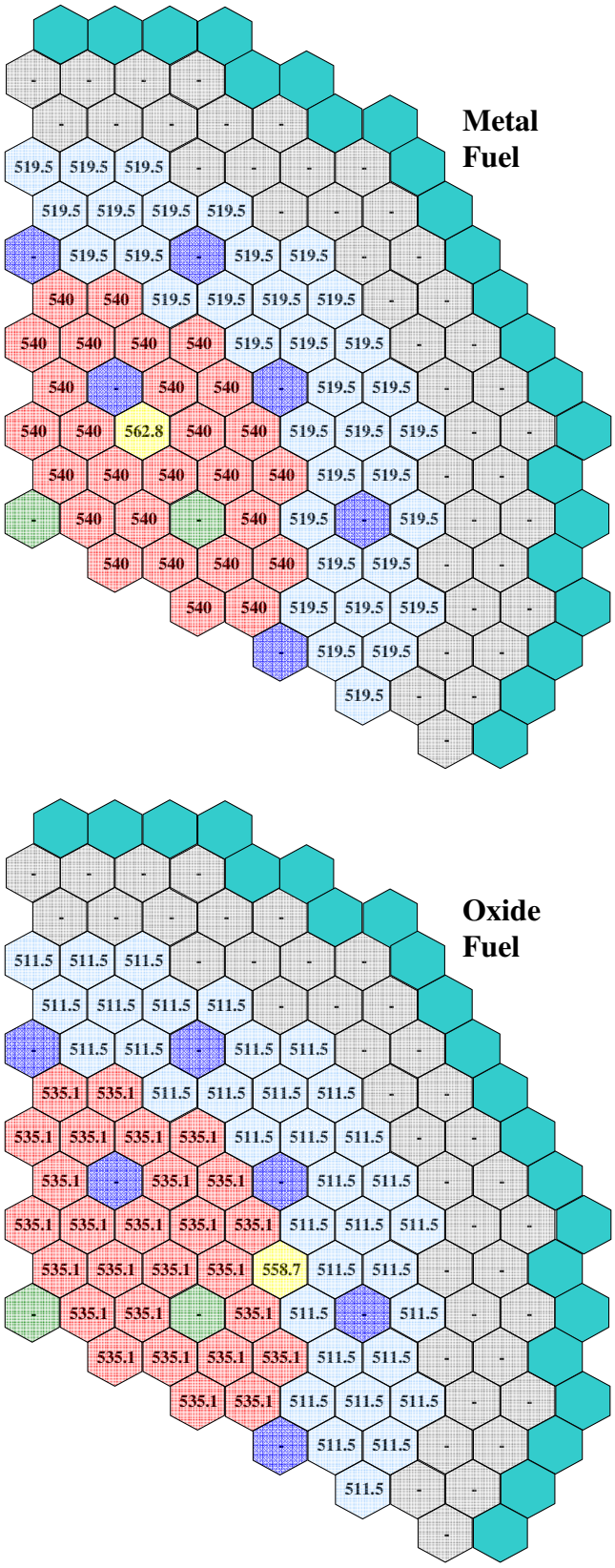

Figure III.7-7: BOEC Initial Peak Cladding Temperature (°C)

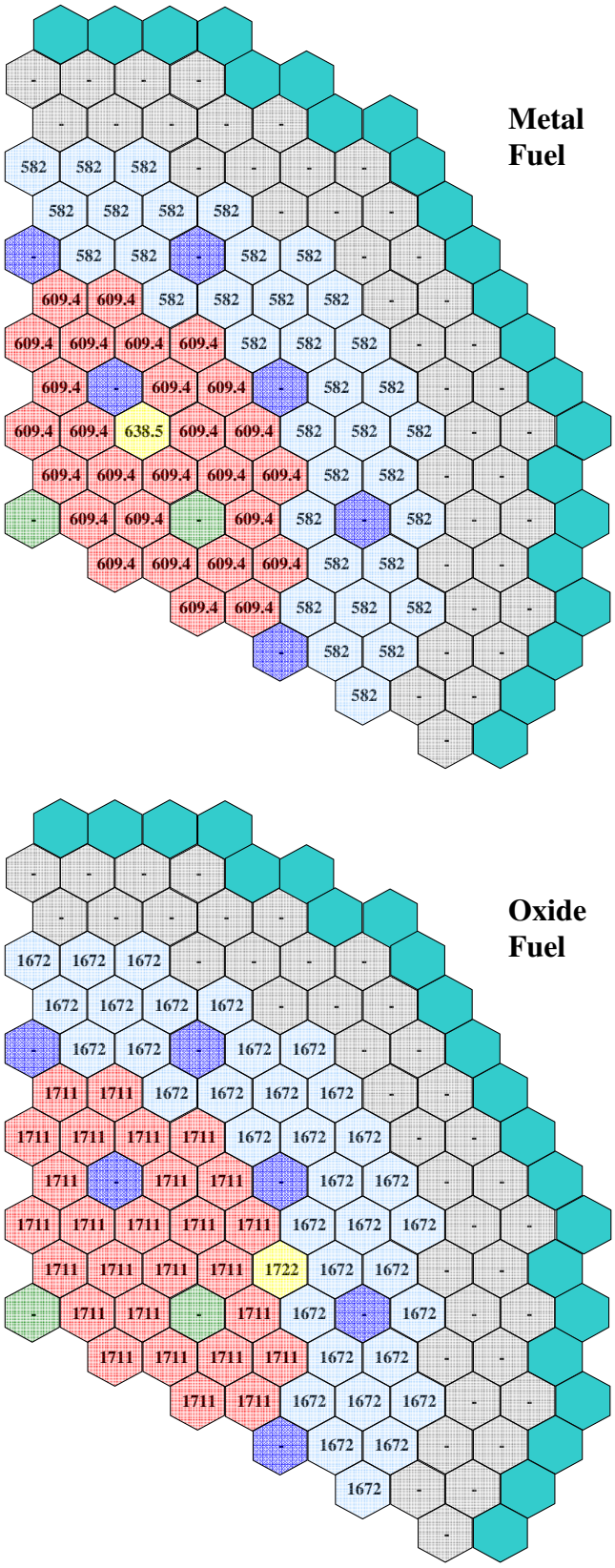

Figure III.7-8: BOEC Initial Peak Fuel Temperature (°C)

III.7.3.2 Coolant Systems Thermal Hydraulics

The coolant systems thermal hydraulics model represents coolant flow and heat transfer in the primary and intermediate sodium systems, and in the emergency decay heat removal system, with a network of volumes and components connected by flow paths. The coolant systems model is shown in Figure III.7-9. From the inlet plenum, cold coolant flows through the core and is heated, then exits to the outlet plenum and travels through the shell side of the intermediate heat exchangers (IHXs), where it gives up its heat. Cold primary coolant exits the IHXs and flows to the cold pool. The primary coolant pumps take suction from the cold pool and deliver the coolant back to the inlet plenum. Emergency decay heat removal is provided by the direct reactor auxiliary cooling system (DRACS), a natural circulation system that removes heat by means of a heat exchanger in the upper region of the primary circuit cold leg and rejects heat through an air dump heat exchanger outside the containment. The working fluid in the DRACS system is NaK.

In the primary coolant circuit, volumes 1 and 2 represent the inlet and outlet plenums. Volumes 3, 4, and 5 represent regions of the cold pool. Volume 3 represents the annular region between the redan and the vessel wall. Volume 4 represents the coolant below and around the inlet plenum. The coolant in volume 4 is essentially stagnant. Volume 5 represents the bulk of the cold pool. Volumes 6 and 9 simulate the gas expansion volumes in the intermediate loop and decay heat removal system, respectively. Volumes 7 and 8 represent the sodium in the active part of the steam generator. Design parameters assumed for the volumes in the model are shown in Table III.7-II. All of the volumes in the model are perfectly mixed (i.e. characterized by a single temperature) except for volumes 2 and 5 which are treated by a stratification model for low flow conditions. Most of the temperature stratification in the system is expected to occur in volumes 2 and 5.

Volumes in the model are connected by one-dimensional flow segments, which are further subdivided into temperature elements for heat transfer calculations. Table III.7-III shows the parameters assumed for the liquid segments. Flow segment 1 stands for the core channels, and flow segment 2 represents the shell side of the IHX. The ABR has four IHXs, but only a single IHX is modeled, and it is assumed in this work that all primary circuits behave identically. Segment 3 represents the four primary coolant pumps and the discharge pipes connected to the inlet plenum. Segment 4 represents the primary coolant flow path through the decay heat removal heat exchanger. Segment 5 connects the annular part of the cold pool with the main part, and segment 6 connects the main region of the cold pool with the near stagnant lower region. Segments 7, 8 and 9 represent the intermediate heat transfer loop including the loop piping, the intermediate heat exchanger, the steam generator and the intermediate coolant pump. Segment 10 represents natural circulation flow in the DRACS loop. In normal operation, heat addition takes place in segment 1, and heat is rejected in segments 2 and 4. Segment 2 is thermally connected through the IHX to the intermediate loop, and segment 4 is thermally connected to the DRACS loop through the DRACS heat exchanger.

In the model, liquid flow segments are divided into a number of elements for the purpose of heat transfer and pressure drop calculations. The liquid elements in the coolant systems model are described in Table III.7-IV.

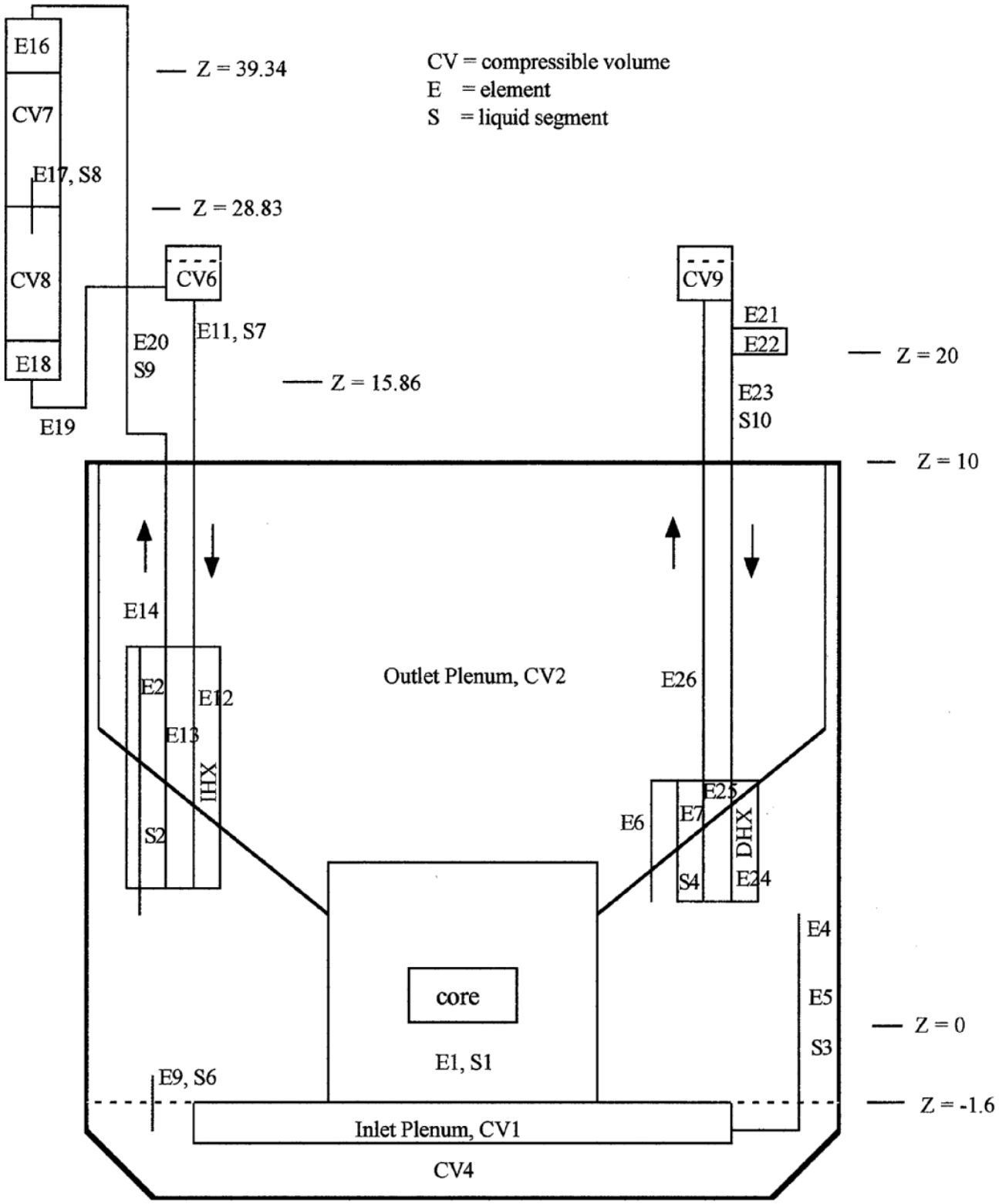

Figure III.7-9: Coolant Systems Thermal Hydraulics Model

Primary and intermediate circuit flows are driven by both forced circulation at the pumps and by buoyancy due to temperature-induced density changes. Transient natural circulation flows adjust to changes in heat generation and heat transfer. DRACS loop natural circulation flow changes due to temperature changes in the DRACS heat exchanger and in the air dump heat exchanger. Heat transfer at the air dump heat exchanger can be enhanced by opening air flow dampers, which are closed during normal operation.

Table III.7-II: PRIMAR-4 Compressible Volumes Input Data.

Compressible Volume	Description	Total Volume m^3	Gas Volume m^3
1	Inlet plenum	7.7	0.
2	Outlet plenum, stratified	895.9	140.
3	Cold pool annulus	76.4	26.7
4	Cold pool, stagnant region below the inlet plenum	1.64	0.
5	Bulk of cold pool, stratified	581.8	0.
6	Intermediate loop expansion volume	20.	10.
7	Sodium in upper half of active region of the steam generator	38.	0.
8	Sodium in lower half of active region of the steam generator	38.	0.
9	Expansion volume in DRACS loop	4.	2.

Table III.7-III: PRIMAR-4 Liquid Segments Input Data.

Segment Number	Elements	Initial Coolant Flow Rate kg/s
1 (core)	1	5029.2
2	2-3	1257.3
3	4-5	1257.3
4	7	0.
5	8	0.
6	9	0.
7	11-16	1290.
8	17	1290.
9	18-20	1290.
10	21-26	0.

Table III.7-IV: PRIMAR-4 Liquid Elements Input Data.

Element	Usage	Inlet Elevation m	Outlet Elevation m	Length m	Area m^2	Hydraulic Diameter	Orifice Coef.
1	Core channels	-1.6	2.973	4.573	(See Table III.7-I)		
2	IHX, shell side	7.31	2.53	4.780	1.044	.0186	15.9
3	IHX outlet	2.53	1.813	.717	.79	1.0	1.0
4	Primary pump	2.016	2.016	.10	.255	.57	0.
5	Pipe	2.016	-1.65	4.0	.255	.57	1.6
6	DRACS inlet annulus	2.6	4.783	2.	.0807	.13	1.6
7	DRACS shell side	4.783	2.263	2.5	.0807	.0491	0.
8	pipe	2.75	2.650	.1	.2	.2	0.
9	pipe	-1.55	-1.65	.1	.2	.2	0.
10	Intermediate pump	23.58	23.58	.1	.25	.5	0.
11	pipe	23.58	7.310	25.	.255	.57	0.
12	pipe	7.31	2.53	4.78	.255	.57	0.
13	IHX, tube side	2.53	7.31	4.78	.7048	.0141	0.
14	pipe	7.31	10.0	6.8	.255	.57	0.
15	pipe	10.0	42.36	76.	.255	.57	0.
16	pipe, SG inlet section	42.36	39.34	3.0	5.2	1.	0.
17	steam generator	28.88	28.78	.1	.255	1.	1.3
18	pipe, SG outlet section	15.86	15.86	3.0	5.2	1.0	0.
19	pipe	15.86	15.86	6.8	.255	.57	0.
20	pipe	15.86	24.88	30.	.255	.57	0.
21	pipe	22.	21.	1.0	.255	.2	0.
22	air dump heat exchanger	21.	20.	11.3	.255	.035	0.
23	pipe	20.	4.763	27.	.255	.2	0.
24	pipe	4.763	2.263	2.5	.255	.2	0.
25	DRACS, tube side	2.263	4.763	2.5	.255	.0204	0.
26	pipe	4.763	22.	30.	.255	.2	1.5

III.7.3.3 Reactor Kinetics and Reactivity Feedback

A point kinetics model is employed to calculate the response of reactor fission power to transient reactivity feedbacks as well as to reactor scram conditions. At any time, the net reactivity is the sum of a number of individual reactivity feedbacks that are determined by the transient thermal, hydraulic, mechanical, and neutronic state of the reactor. The feedback reactivities considered are fuel Doppler, coolant density, fuel and cladding axial expansion, radial core expansion, and control rod driveline thermal expansion. In addition to tracking fission power, a decay heat model is integrated with the point kinetics model to track thermal power in sub-critical conditions.

Fuel Doppler feedback is calculated from the spatially-dependent fuel temperature distribution and the input spatial distribution of the fuel Doppler reactivity coefficient. In each single-pin channel, the axial distribution of the radial pin-average fuel temperature is used to calculate the reactivity feedback.

Coolant density reactivity feedback is calculated from the spatially dependent coolant density distribution and the input distribution of the coolant density reactivity coefficient calculated from perturbation theory. The reactivity feedback data is entered as a coolant void worth (the negative of the coolant mass worth).

Transient fuel and cladding temperatures are used to predict fuel and cladding axial dimension changes, and in each single-pin channel the reactivity feedbacks associated with fuel and cladding axial expansion are computed from first order perturbation theory.

A simple radial core expansion model accounts for core dilation due to thermal expansion of the above-core load pads and thermal expansion of the core support grid plate. Reactivity feedback is then calculated from the computed core dimension change and an input linear reactivity coefficient based on stand-alone reactor physics eigenvalue calculations.

For the control-rod driveline feedback model, it is assumed that the control rod drivelines are washed by the outlet coolant from the core. Thermal expansion of the drivelines due to a rise in core outlet temperature will cause the control rods to be inserted further into the core, providing a negative reactivity component. On the other hand, when the control rod drives are supported on the vessel head and the core is supported by the vessel walls, then heating the vessel walls will lower the core, leading to a positive reactivity component. In the present model, both control-rod driveline expansion and vessel wall expansion are treated.

For the parametric variation on the oxide core design where a self-actuated shutdown system (SASS) is employed, the analysis here assumes the presence of a safety rod passive de-latch mechanism utilizing magnetic resistance change at the Curie point temperature of the sensing alloy. The SASS is assumed to be coupled to the secondary control-rods with a total scram worth of $8.7. The insertion is initiated by the coolant outlet temperature of channel 1 (inner driver subassembly) reaching 727°C (1000K).

III.7.4 Analysis Results

Analyses of the protected loss-of-flow (PLOF) and unprotected loss-of-flow (ULOF) accident sequences were performed with coupled heat transfer, thermal-hydraulics, and

reactor kinetics models available in the SAS4A/SASSYS-1 code. These models have been validated through many applications to EBR-II and FFTF transient tests. Additionally, temperature criteria for assessments of cladding damage thresholds have been established by results from testing of fuel in EBR-II, TREAT, and FFTF. Consequently, there is high confidence that the detailed results from the PLOF and ULOF accident analyses presented here give a true characterization of the physical performance that could be obtained in the ABR design.

The base case results for both metal and oxide core designs are for the beginning of equilibrium cycle conditions. Detailed analysis results for the PLOF and ULOF accident sequences are presented below. In addition to the base cases, parametric variations have also been performed for the ULOF accident sequence for both the metallic-fueled and the oxide-fueled cores. Parametric variations for the metal core involve changes to the control-rod driveline (CRDL) expansion reactivity feedback. Parametric variations for the oxide core also involve the CRDL reactivity feedback, but additional results are presented for the case where a self-actuated shutdown system (SASS) is employed. The SASS could be a secondary or a tertiary shutdown system. The specific SASS device selected for the analysis presented here is based on a safety rod passive de-latch mechanism utilizing magnetic resistance change at the Curie point temperature of the sensing alloy.

III.7.4.1 Metal Fuel

Protected Loss-of-Flow (PLOF) Accident Sequence

Results from analysis of the metal fuel PLOF accident sequence are shown in Figures III.7-10, III.7-11, III.7-12, and III.7-13. Figures III.7-10 and III.7-11 show the history of the reactor power, the decay heat power, the DRACS heat removal rate and the coolant flows through the highest temperature subassembly (channel 4) and an average temperature subassembly (channel 1) in the inner core. This transient is initiated by a complete loss of forced coolant flow in the primary and intermediate loops, and is driven in the early transient period largely by the pump coast-down. During the later period when a long-term quasi-equilibrium is being reached, the response is driven more by temperature distributions with-in the hot and cold pools and the thermal boundary conditions. The discussion in this section is separated into these two time periods of the transient history. Both the primary pumps and the intermediate pumps have enough inertia to give initial flow halving times of five seconds. Primary pump rotors completely stop turning at about 150 seconds after the start of the transient, leading to a transition to natural circulation. The transition to natural circulation goes as smoothly in the cooler channel 1 as in the hotter channel 4. Almost immediately at initiation, the reactor protection system scrams the reactor, beginning the power reduction to decay heat shown in Figure III.7-10, and the dampers on the DRACS air dump heat exchangers open, permitting the DRACS to operate at its full capacity of 0.5%. As the cold pool temperature rises, DRACS heat removal capacity increases, eventually reaching the equivalent of 0.7% of normal reactor power. Not indicated in this figure is the loss of heat removal to the balance-of-plant, which is assumed to occur after the first 10 seconds. Figure III.7-11 shows that the reactor decay heat power equals the DRACS heat removal capacity at about 6 hours into the transient.

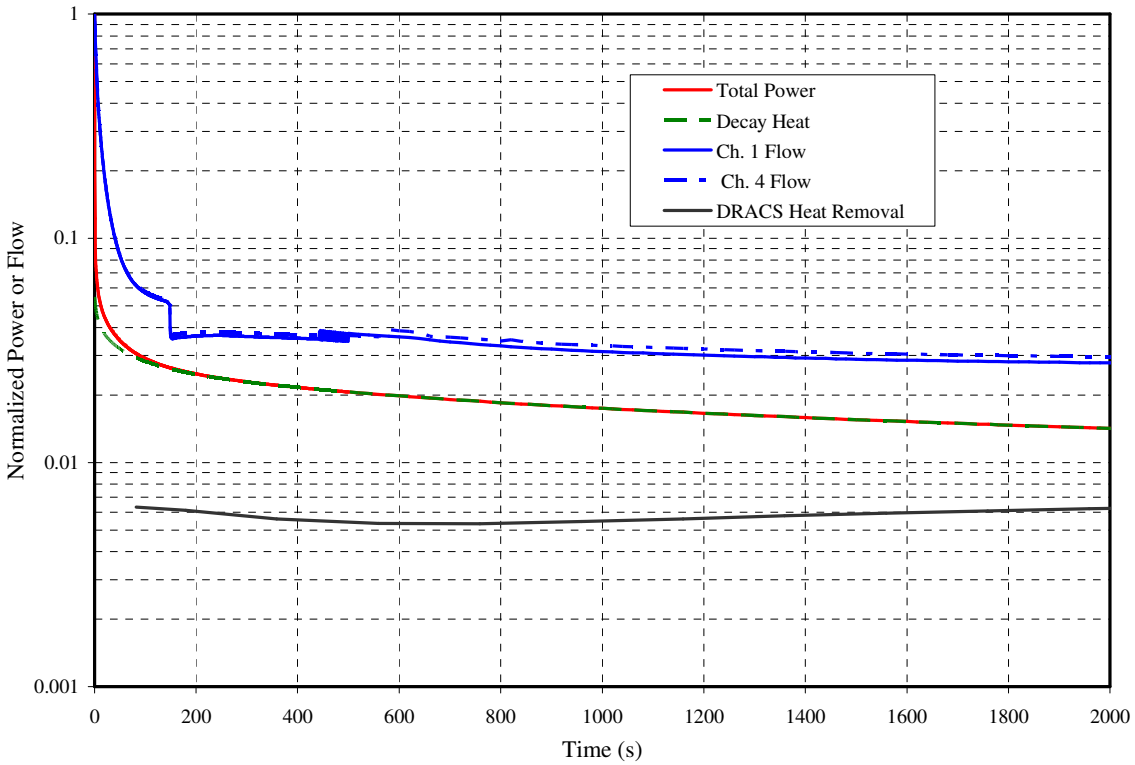

Figure III.7-10: Metal Fuel PLOF Power and Flow History, Early Times

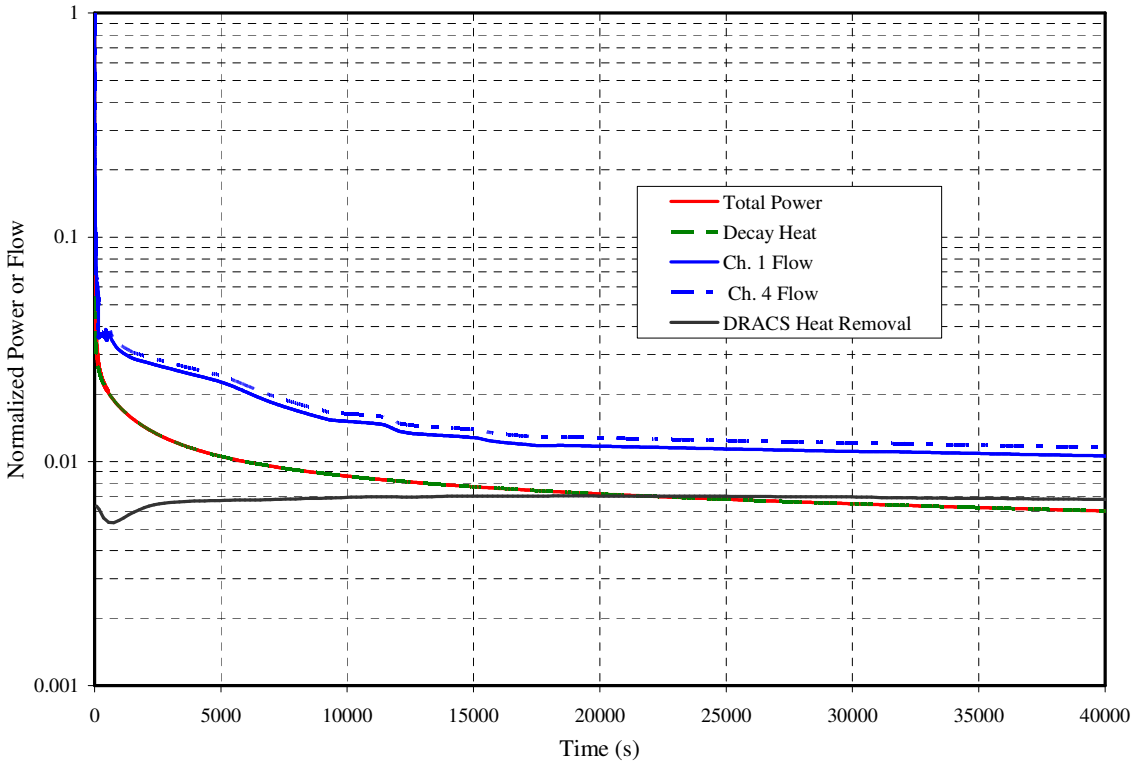

Figure III.7-11: Metal Fuel PLOF Power and Flow History, Extended Times

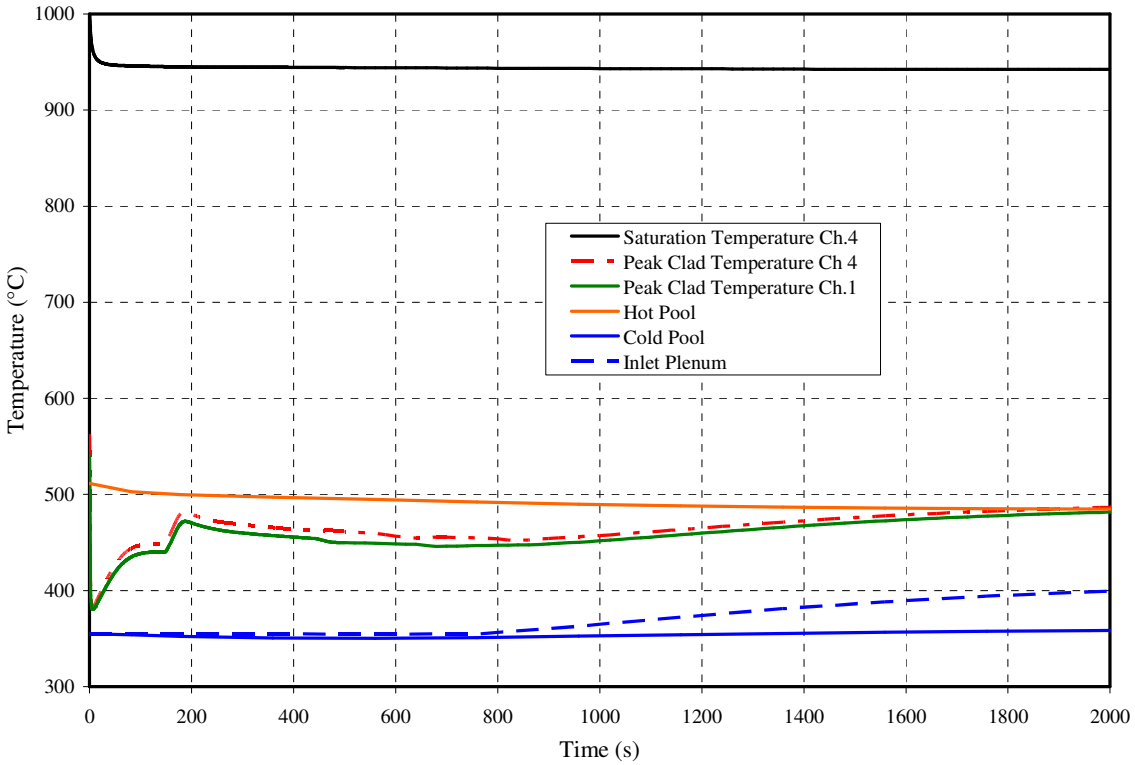

Figure III.7-12: Metal Fuel PLOF Temperature History, Early Times

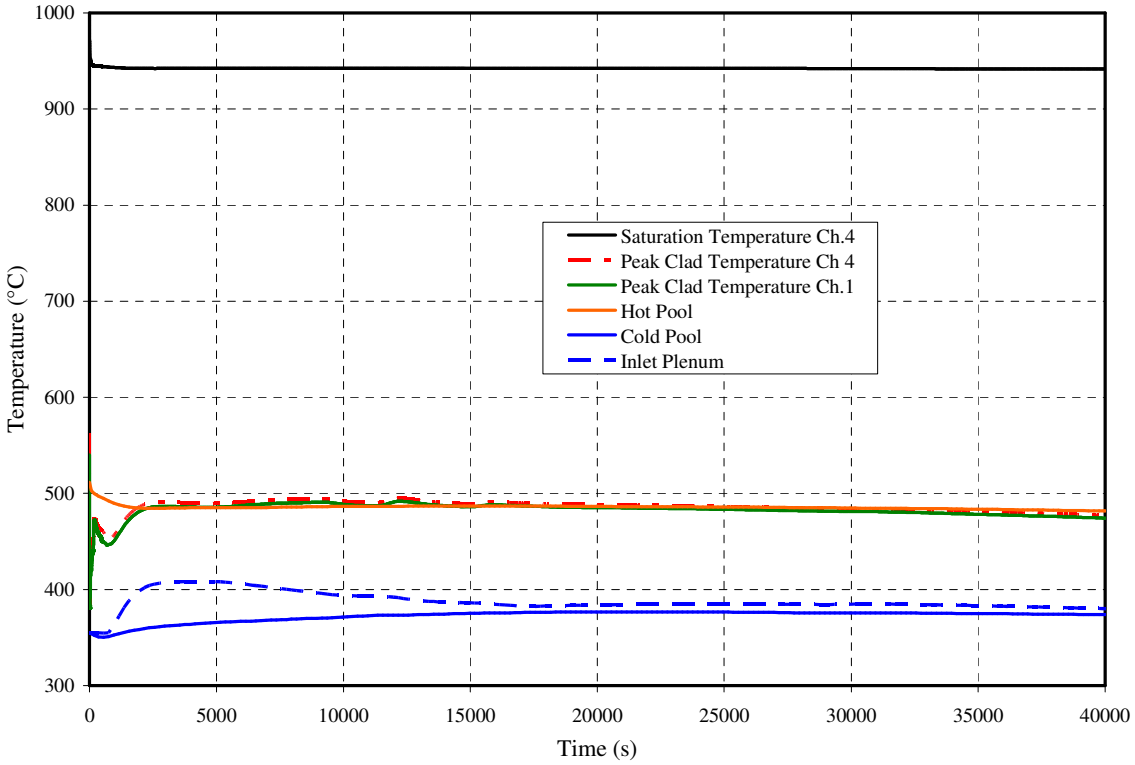

Figure III.7-13: Metal Fuel PLOF Temperature History, Extended Times

Figure III.7-12 shows the early reactor temperature histories during the coolant flow coast down and transition to natural circulation. During this and the following time, the only heat removal is through the DRACS. The rapid reactor power decrease due to the scram initially lowers the coolant and cladding temperatures in the core. Then the drop in core flow as the pumps coast down leads to a rise in core coolant and cladding temperatures. The transition to natural circulation is about as smooth in channel 1 as in channel 4. In both channels as the primary pumps stop turning the coolant flow rate abruptly drops to very low values, leading to higher peak coolant and cladding temperatures at around 180 seconds. This short-term cladding temperature rise however is still lower than the initial peak clad temperatures so no cladding failure would occur. There is a large margin to coolant boiling.

Note that the "cold pool" temperature shown in Figures III.7-12 and III.7-13 is the average temperature of the axial distribution computed with the volume stratification model. The pump inlet is at a certain elevation in the cold pool, and at this location the coolant temperature is different from the average for the cold pool.

In the longer term transient history when the system temperature rises, as shown in Figure III.7-13, the DRACS heat removal capability increases due to an increase in NaK flow and heat rejection at the air dump heat exchangers. Decay heat production declines throughout the transient, until it becomes equal to the DRACS heat removal. Hot pool and cold pool temperatures reach long-term peak values at about this time which is around 6 to 7 hours into the transient, and then uniformly decrease as the whole system cools. The DRACS begins to remove more heat than the decay heat rate production. Channel cladding temperatures follow the inlet plenum temperature history to a large part, as the inlet channel flows start to stabilize and a long-term natural convection quasi-equilibrium is reached. During this period the results show the effect of the stratification within the hot and cold pools on this flow and the channel temperatures in the core.

The significance of the PLOF analysis results is emphasized in Figure III.7-12 which shows the initial peak cladding temperature (563°C) in channel 4, compared to the short-term transient peak cladding temperature of 490°C and the long-term peak cladding temperature just above 470°C at around 5 hours before the cool down begins to take effect. In the PLOF transient, no cladding failures would occur, and the long-term peak temperatures in the accident are lower than the normal operating temperatures. Stated in another way, the long-term temperature safety margins in the accident are greater than the margins at the normal operating conditions. This very significant result is obtained as a result of the natural circulation capabilities of the reactor coolant system and the DRACS.

Unprotected Loss-of-Flow (ULOF) Accident Sequence

a) Base Case

The metal fuel ULOF transient is initiated by the same set of failures as for the PLOF accident (loss of forced flow and loss of normal heat rejection). However, for the ULOF case, the reactor protection system also fails to scram the reactor; so the accident proceeds from full power. All heat rejection is through the DRACS, with a design heat rejection of 0.5% of full power at nominal conditions. Results from the analysis of the ULOF accident sequence are shown in Figures III.7-14, III.7-15, and III.7-16. Similar to the PLOF results, there is an early transient period which is driven mostly by the pump

coast-downs. Then, during a later period when a long-term quasi-equilibrium is being reached, the response is driven more by temperature distributions within the hot and cold pools and the thermal boundary conditions. However, unlike the PLOF case, in these results there is coupling between the power history and the thermal response through the passive core reactivity feedbacks since the core is not shutdown through a scram. This two-way coupling is reflected in the results presented below.

Figure III.7-14 shows the histories for the total reactor power, the decay heat production, and the coolant flow in channel 4 (the peak inner core assembly). The power-to-flow imbalance during the first 50 seconds results in significant transient reactor heating. Peak fuel, peak clad, and coolant outlet temperatures for channel 4 are shown in Figure III.7-15. Coolant and cladding temperatures increase to approximately 700°C within the first 30 seconds. The fuel temperature increases to about 730°C. This heating causes the reactivity feedbacks shown in Figure III.7-16. The net reactivity reaches 80 cents sub-critical. Control-rod driveline (CRDL) and radial expansion are the main contributors to the initial negative reactivity feedback, which causes power and fuel temperatures to decline. Shortly after the onset of the transient, higher-temperature coolant begins washing over and heating the control-rod drivelines. As the drivelines expand, an additional negative reactivity component is introduced, as shown in Figure III.7-16. Although reduced fuel temperatures provide a positive Doppler feedback, the magnitude is modest due to the high thermal conductivity and relatively low operating temperatures of metallic fuel. As a consequence, by 100 seconds the total power is significantly below 10% nominal. The power-to-flow ratio initially increases, but due to the net negative reactivity, peaks and then decreases. Beyond 1000 seconds, the power-to-flow ratio remains below one for the duration of the transient.

The flow coast-down provided by the inertia of the primary pumps ends at approximately 150 seconds when the shafts stop turning. At this point, natural circulation has not yet been fully established, so with the abrupt drop in flow the cladding and local coolant temperatures begin to rise to form a second temperature peak of about 550°C at approximately 200 to 250 seconds. The increased temperatures provide additional driving force to aid in establishing natural circulation flow. But the second temperature peak also causes additional thermal expansion and negative reactivity feedback and this starts a period of oscillations between the fission power and the thermal hydraulic feedback effects. The oscillations are damped oscillations and the conditions eventually reach a quasi-equilibrium. By 2000 seconds, fission power has been significantly reduced, and residual heating is dominated by decay heat. Therefore, the changes in reactivity feedback (particularly CRDL expansion) have negligible impact on subsequent transient development.

As natural circulation is being established, and with changes in the channel inlet temperatures, the peak in the coolant temperature moves up through the core and to the subassembly outlet. Similarly, the delay in observing the temperature peak at the outlet is partly due to the low flow conditions, but a bigger contributor to the delay is the large thermal inertia of the structural materials above the core, which must all be heated before the temperature peak reaches the outlet. This affects the hot pool temperature distributions for establishing a quasi-equilibrium natural circulation. But the development of natural circulation holds peak coolant and cladding temperatures to around 520°C. The

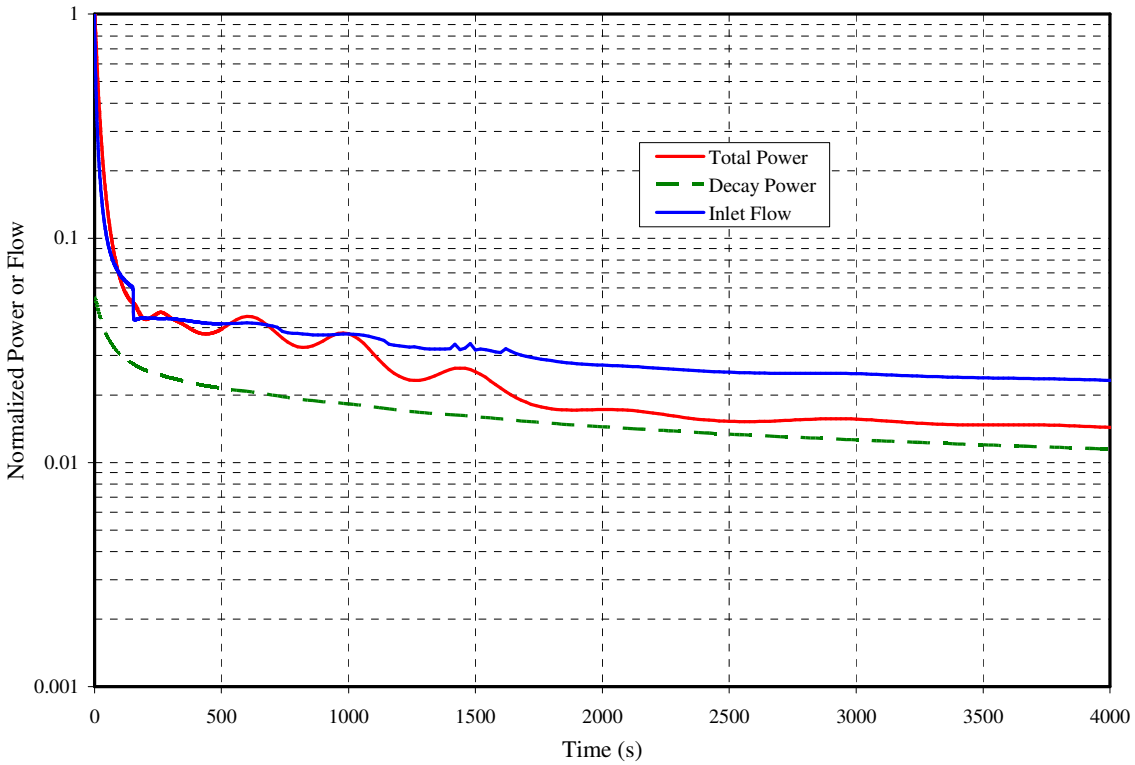

Figure III.7-14: Metal Fuel ULOF Transient Total Power and Channel 4 Flow

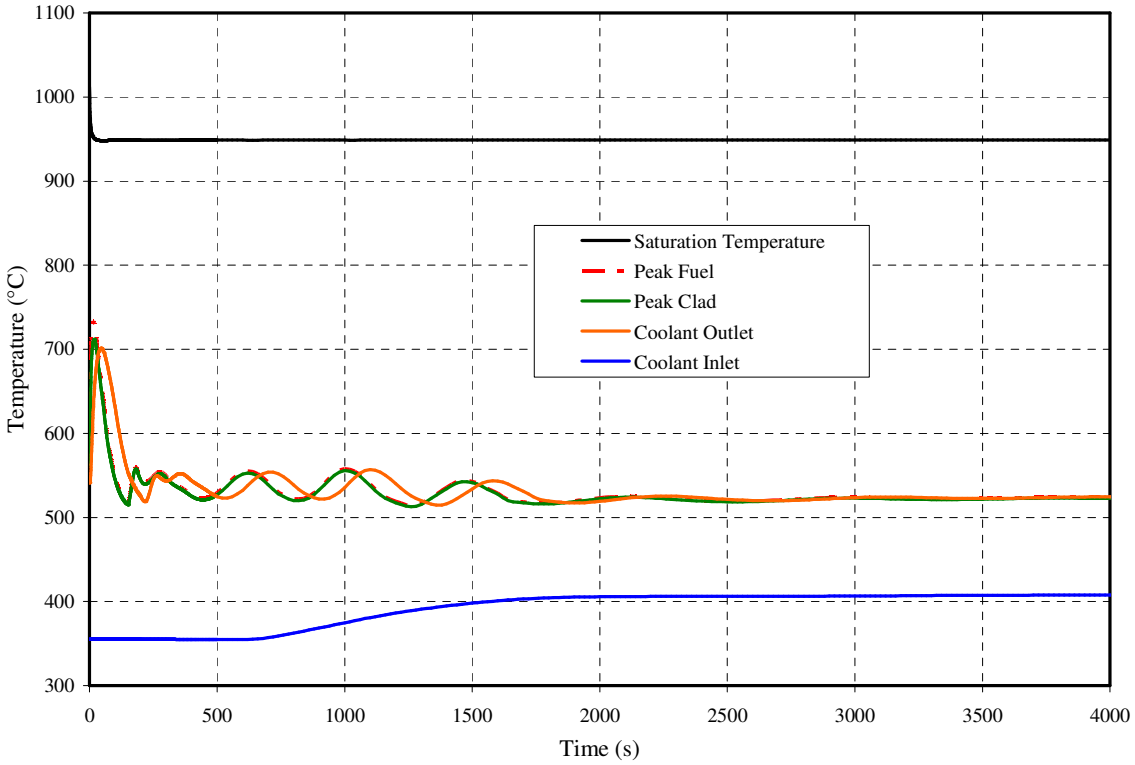

Figure III.7-15: Metal Fuel ULOF Transient Temperatures for Channel 4

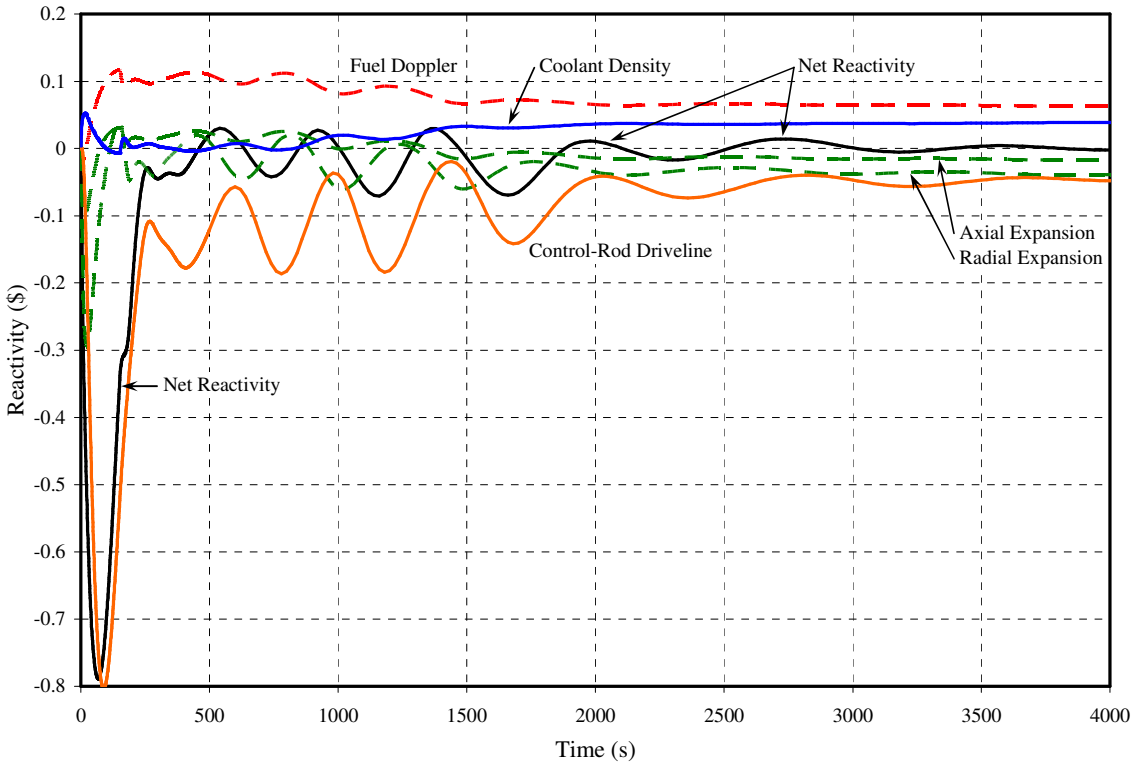

Figure III.7-16: Metal Fuel ULOF Transient Reactivity Feedback

peak fuel temperatures follow. Beyond 6000 seconds, the normalized power-to-flow remains quasi-constant, and the channel temperatures do not increase significantly but are driven by the inlet core temperature as the system slowly heats up. In the long term beyond 20,000 seconds, when the total power approaches the heat rejection capability of the DRACS, overall system temperature rise begins to level off.

The significance of the ULOF accident analysis results for the metal-fueled core is confirmed by Figure III.7-15. As shown for channel 4, the peak fuel, cladding, and coolant temperatures remain well below the coolant saturation (boiling) temperature, with a minimum margin to coolant boiling of about 250°C. The analysis suggests that the core would survive an unprotected loss-of-flow accident without pin failures or fuel damage. This very favorable result comes about because of 1) the high thermal conductivity and relatively low operating temperature of metallic fuel, 2) the capability of a sodium-cooled reactor in a pool-type primary system to remove decay heat in natural circulation, and 3) the beneficial negative reactivity feedback coefficients and reactor physics performance of metallic fuel.

b) Reduced CRDL Feedback Case

A parametric variation has been performed for the metal-fueled core with reduced CRDL feedback. Reference should be made to the discussion above for the base case (a). In this parametric, the worth fitting coefficients for the CRDL expansion feedback model have also been reduced from the metal-fueled core base case (a) by 50%. This is approximately equivalent to reducing the worth by a factor of two and could be viewed as more appropriate for an EOEC case with the rods withdrawn. The ULOF transient is

initiated by the same set of failures as for the base case (loss of forced flow and loss of normal heat rejection) and the reactor protection system also fails to scram the reactor; so the accident proceeds from full power. All heat rejection is through the DRACS, with a design heat rejection of 0.5% of full power at nominal conditions. Results from the analysis of the ULOF accident sequence are shown in Figures III.7-17, III.7-18, and III.7-19. The same overall trends can be seen when compared with the metal-fueled core base case (a), although the core temperature margins are slightly reduced.

Figure III.7-17 shows the histories for total reactor power, decay heat production, and coolant flow in channel 4 (the peak inner core assembly). The power-to-flow imbalance during the first 50 seconds results in significant transient reactor heating. Peak fuel, peak clad, and coolant outlet temperatures for channel 4 are shown in Figure III.7-18. Coolant and cladding temperatures increase to approximately 720°C within the first 30 seconds. The fuel temperature reaches 740°C. These temperatures are all slightly higher than the metal-core base case. This heating causes the reactivity feedbacks shown in Figure III.7-19. As with the base case, CRDL and radial expansion are the main contributors to the initial negative reactivity feedback, which causes power and fuel temperatures to decline. As can be anticipated, the CRDL feedback is reduced in comparison to the base case though the reduction is not proportionate to the assumed reduction in the worth fitting coefficients. Reduced fuel temperatures provide a positive Doppler feedback, although the magnitude is modest due to the high thermal conductivity and relatively low operating temperatures of metallic fuel. The magnitude of this feedback component is quite similar to that of the base case. Consistent with these feedbacks, the total power is slightly higher at this point in the transient.

The flow coast-down provided by the inertia of the primary pumps ends at approximately 150 seconds when the shafts stop turning. As in the base case, natural circulation has not yet been fully established, so with the abrupt drop in flow the fuel, cladding, and local coolant temperatures begin to rise to form a second temperature peak of about 560°C at approximately 180 to 200 seconds. The increased temperatures provide additional driving force to aid in establishing natural circulation flow. But as in the base case, the second temperature peak also causes additional thermal expansion and negative reactivity feedback and this starts a period of oscillations between the fission power and the thermal hydraulic feedback effects. However, the oscillations are damped significantly faster and the conditions reach a quasi-equilibrium much sooner than in the base case. By 2000 seconds, fission power has been significantly reduced, and residual heating is dominated by decay heat. Therefore changes in reactivity feedback (particularly CRDL expansion) have negligible impact on subsequent transient development.

As a consequence, during the quasi-equilibrium phase as natural circulation is being established, the same behavior as in the base case can be observed and reference should be made to that discussion. The development of natural circulation holds peak coolant and cladding temperatures to around 520°C. The peak fuel temperatures follow. Beyond 6000 seconds, the normalized power-to-flow remains quasi-constant and the channel temperatures do not increase significantly. In the long term beyond 20000 seconds, the total power approaches the heat rejection capability of the DRACS, and the overall system temperature rise begins to level off.

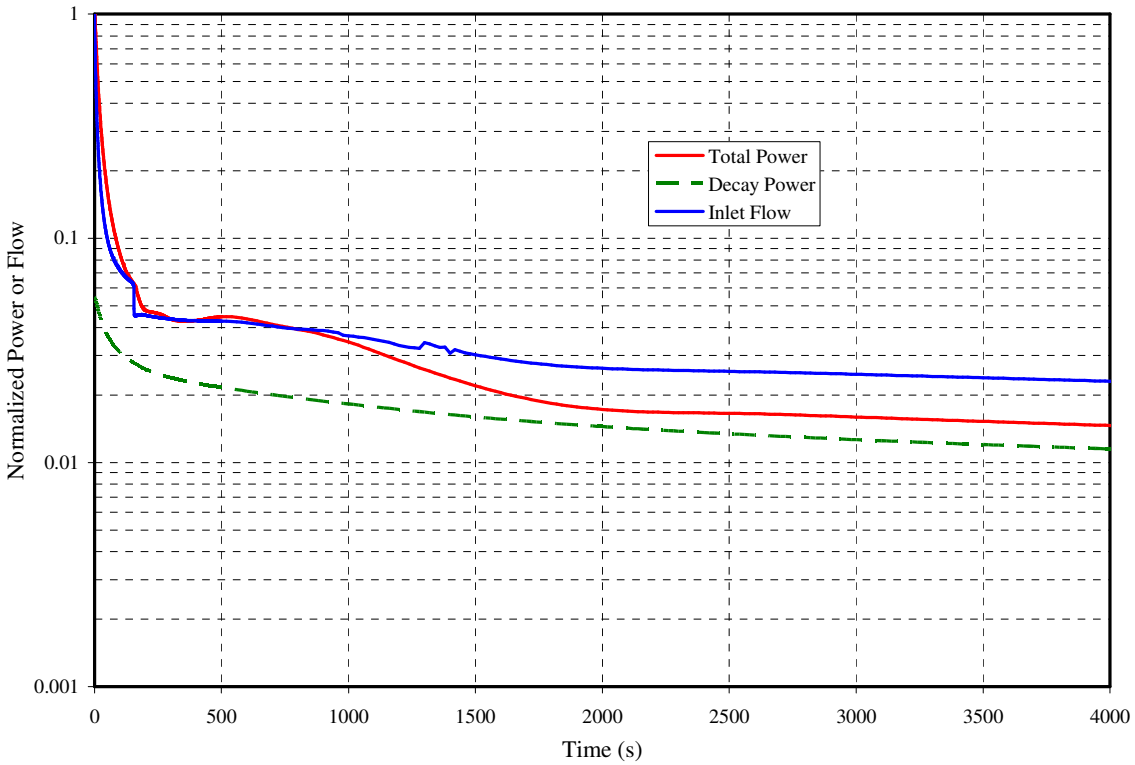

Figure III.7-17: Metal Fuel ULOF Transient Total Power and Channel 4 Flow (50% CDRL Feedback)

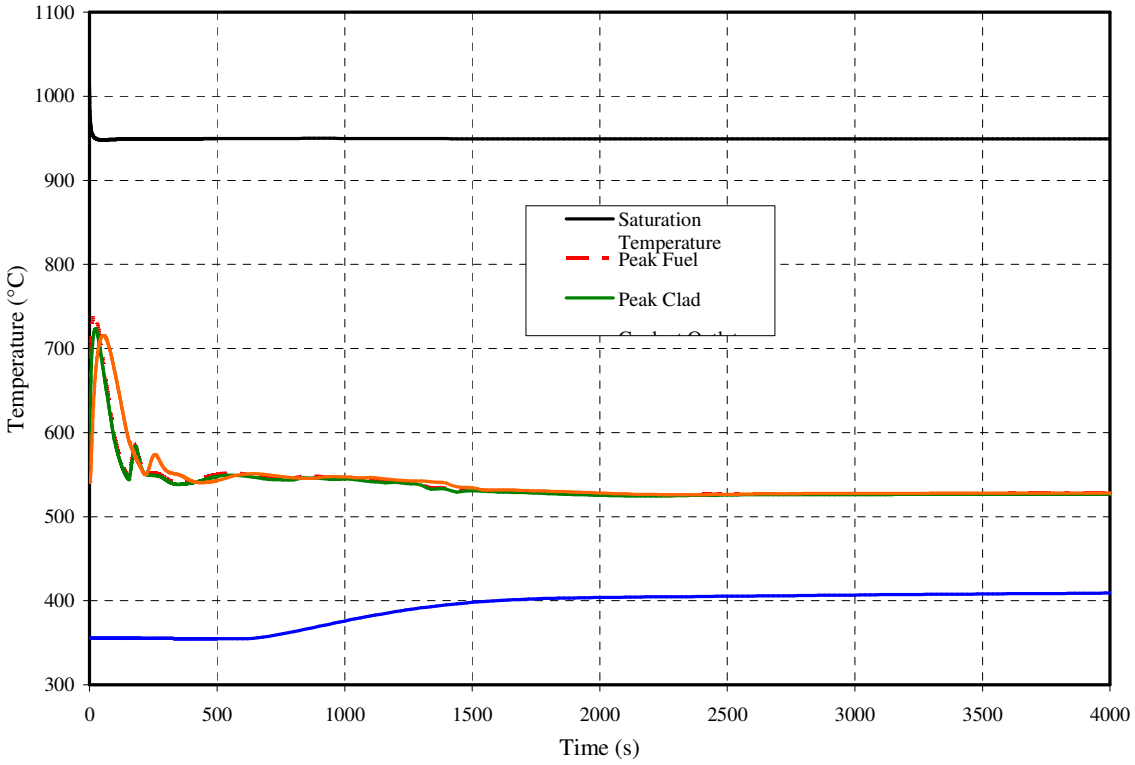

Figure III.7-18: Metal Fuel ULOF Transient Temperatures for Channel 4 (50% CDRL Feedback)

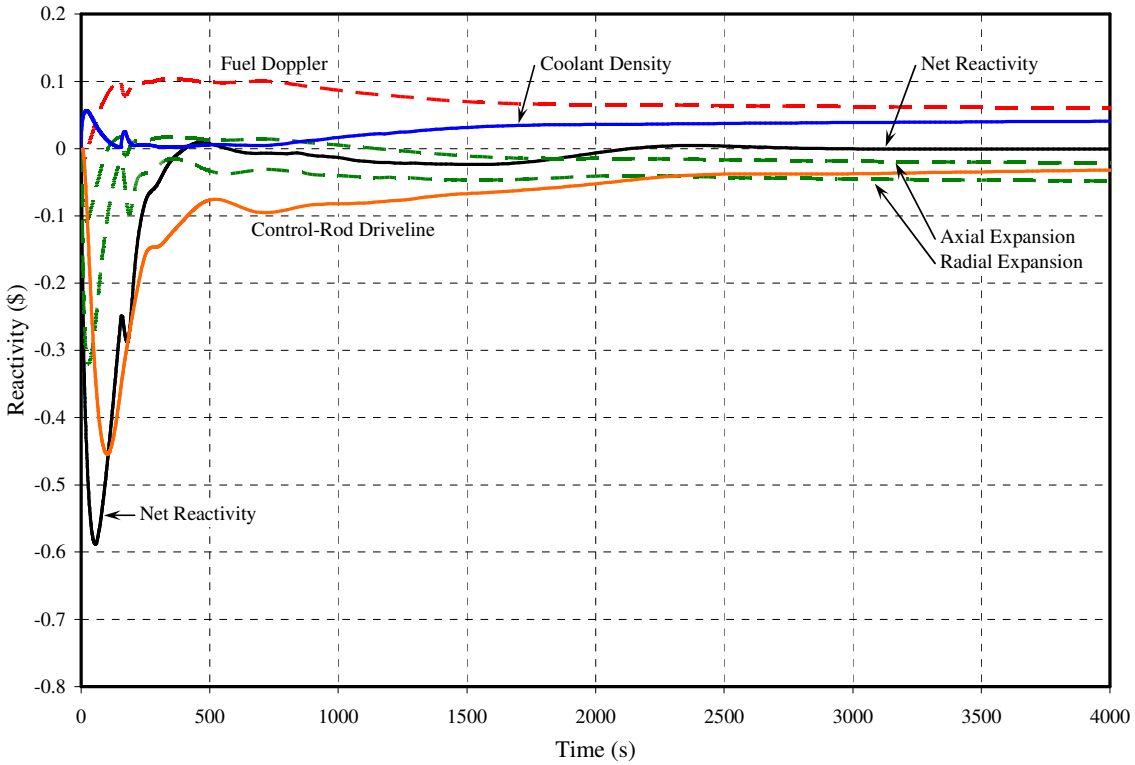

Figure III.7-19: Metal Fuel ULOF Transient Reactivity Feedback
(50% CDRL Feedback)

The significance of these ULOF accident analysis results for the reduced CRDL feedback is that the margins are only slightly different from those of the metal-fueled core base case (a). A change of 50% only affects the large margins by about 20°C. This is confirmed in Figure III.7-18. As shown for channel 4, the peak fuel, cladding, and coolant temperatures remain well below the coolant saturation (boiling) temperature, and the minimum margin to coolant boiling is about 220°C. The conclusions for the base case are still valid here. The metal-fueled core would survive an unprotected loss-of-flow accident without pin failures or fuel damage. As with case (a), this very favorable result comes about because of 1) the high thermal conductivity and relatively low operating temperature of metallic fuel, 2) the capability of a sodium-cooled reactor in a pool-type primary system to remove decay heat in natural circulation, and 3) the beneficial negative reactivity feedback coefficients and reactor physics performance of metallic fuel.

III.7.4.2 Oxide Fuel

Protected Loss-of-Flow (PLOF) Accident Sequence

Results from analysis of the oxide fuel PLOF accident sequence are shown in Figures III.7-20, III.7-21, III.7-22, and III.7-23. Figures III.7-20 and III.7-21 show the history of the reactor power, the decay heat power, the DRACS heat removal rate and the coolant flows through the highest temperature subassembly (channel 4) and an average temperature subassembly (channel 1) in the inner core. This transient is initiated by a complete loss of forced coolant flow in the primary and intermediate loops, and is driven

in the early transient period largely by the pump coast-down. The later period when a long-term quasi-equilibrium is being reached, the response is driven more by temperature distributions within the hot and cold pools and the thermal boundary conditions. The discussion in this section is separated into these two time periods of the transient history. The primary pumps are assumed to have enough inertia to give initial flow halving times of 20 seconds. The intermediate pump inertia is sufficient for an initial flow halving time of five seconds. The primary pump rotors completely stop turning at about 650 seconds after the start of the transient, leading to a transition to natural circulation. The transition to natural circulation goes as smoothly in the cooler channel 1 as in the hotter channel 4. Almost immediately at initiation, the reactor protection system scrams the reactor, beginning the power reduction to decay heat shown in Figure III.7-20, and the dampers on the DRACS air dump heat exchangers open, permitting the DRACS to operate at its full capacity of 0.5%. As the cold pool temperature rises, DRACS heat removal capacity increases, eventually reaching the equivalent of 0.7% of normal reactor power. Not indicated in this figure is the loss of heat removal to the balance-of-plant, which is assumed to occur after the first ten seconds. Figure III.7-21 shows that the reactor decay heat power equals the DRACS heat removal capacity at about six hours into the transient.

Figure III.7-22 shows the early reactor temperature histories during the coolant flow coast down and transition to natural circulation. During this and the following time, the only heat removal is through the DRACS. The rapid reactor power decrease due to the scram initially lowers the coolant and cladding temperatures in the core. The total power history essentially follows the decay heat curve as the fission power is negligible. Then the drop in core flow as the pumps coast down leads to a rise in core coolant and cladding temperatures. The transition to natural circulation is about as smooth in channel 1 as in channel 4, so the temperature behavior in the two channels tends to mirror each other. In both channels as the primary pumps stop turning the inlet coolant flow rate abruptly drops to very low values, leading to higher peak coolant and cladding temperatures at around 680 seconds. This short-term cladding temperature rise is however still lower than the initial peak clad temperatures so no cladding failure would occur. There is a large margin to coolant boiling.

Note that the “cold pool” temperature shown in Figures III.7-22 and III.7-23 is the average temperature of the axial distribution computed with the volume stratification model. The pump inlet is at a certain elevation in the cold pool, and at this location the coolant temperature is different from the average for the cold pool.

In the longer term transient history while the system temperature rises, as shown in Figure III.7-23, the DRACS heat removal capability increases due to an increase in NaK flow and heat rejection at the air dump heat exchangers. Decay heat production declines throughout the transient, until it becomes equal to the DRACS heat removal. Fig III.7-23 shows that this occurs around 6 to 7 hours after the initiation of the transient. The elevated pool temperatures at this time have led to both an increase in the DRACS natural convection flow and in the driving temperature difference to the air dump heat exchangers, which together contribute to the increase in the DRACS heat removal capability over the design value. Hot pool and cold pool temperatures reach long-term peak values at about this time, and then uniformly decrease as the whole system cools. The DRACS begins to remove more heat than the decay heat rate production. Channel

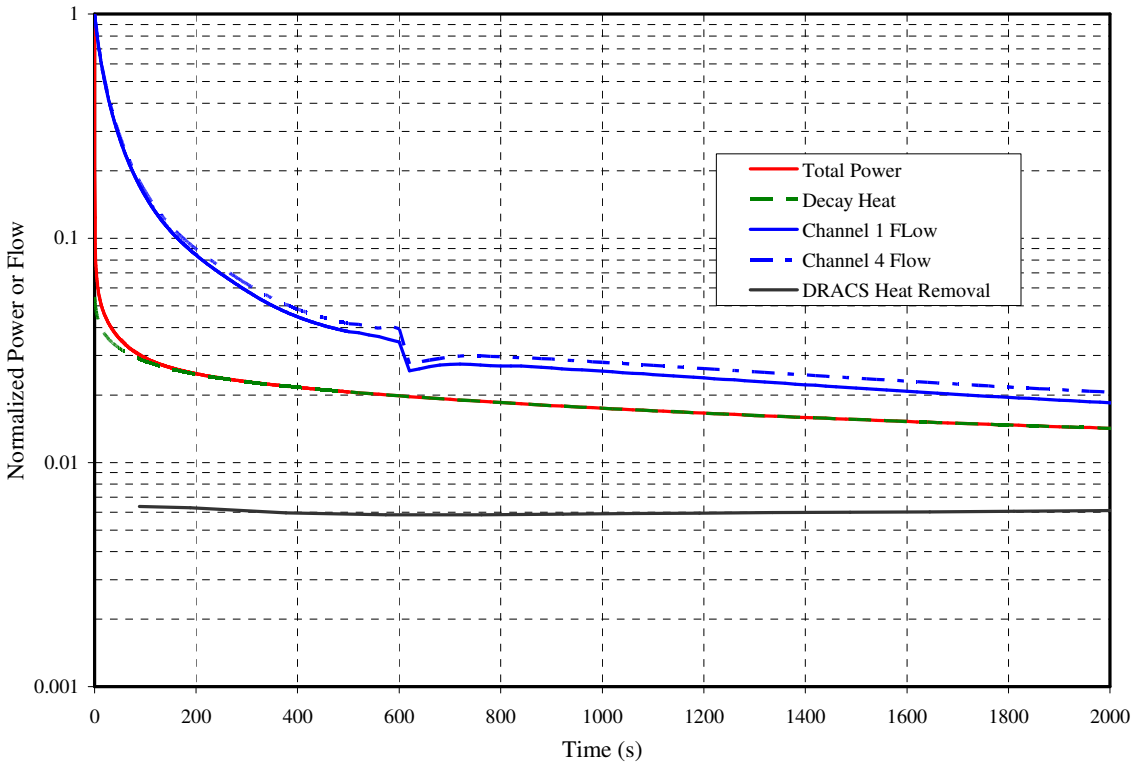

Figure III.7-20: Oxide Fuel PLOF Power and Flow History, Early Times

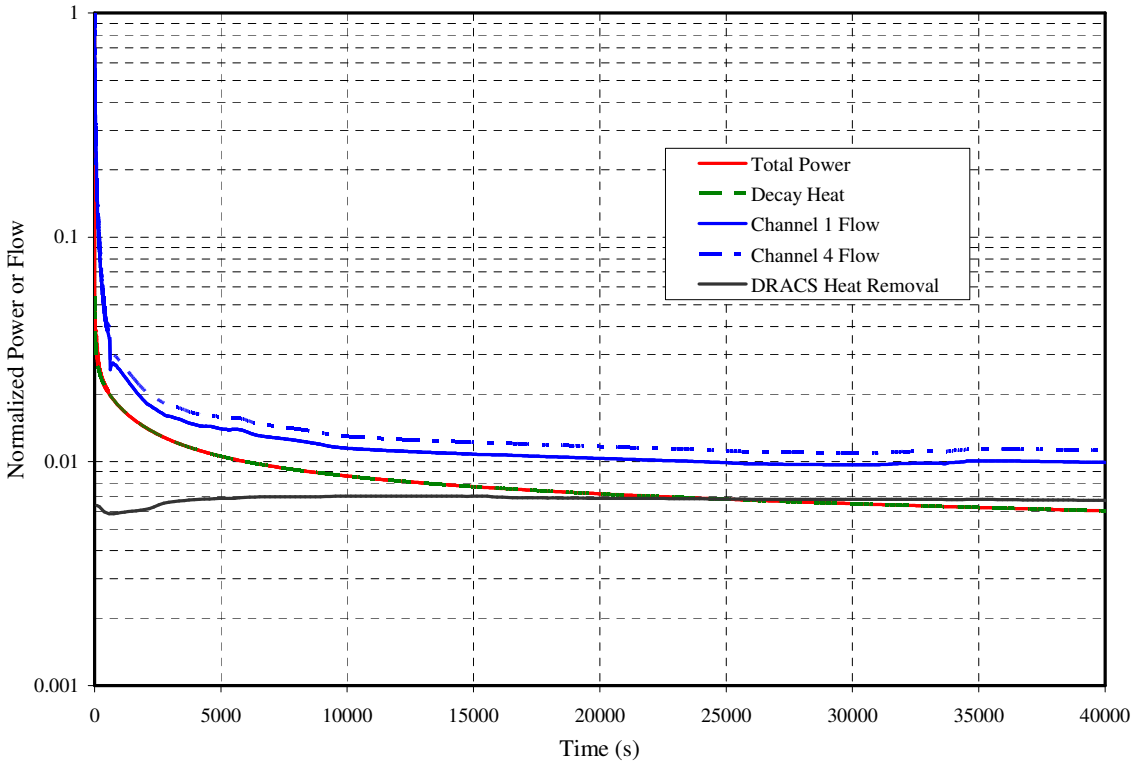

Figure III.7-21: Oxide Fuel PLOF Power and Flow History, Extended Times

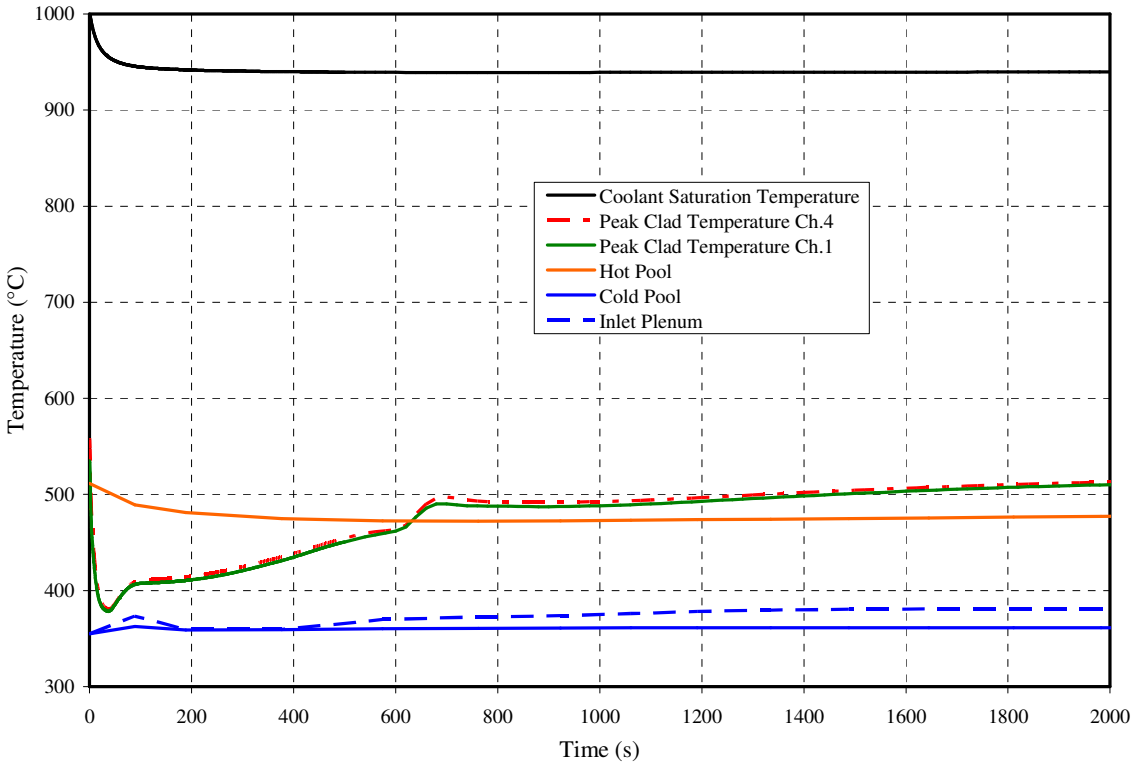

Figure III.7-22: Oxide Fuel PLOF Temperature History, Early Times

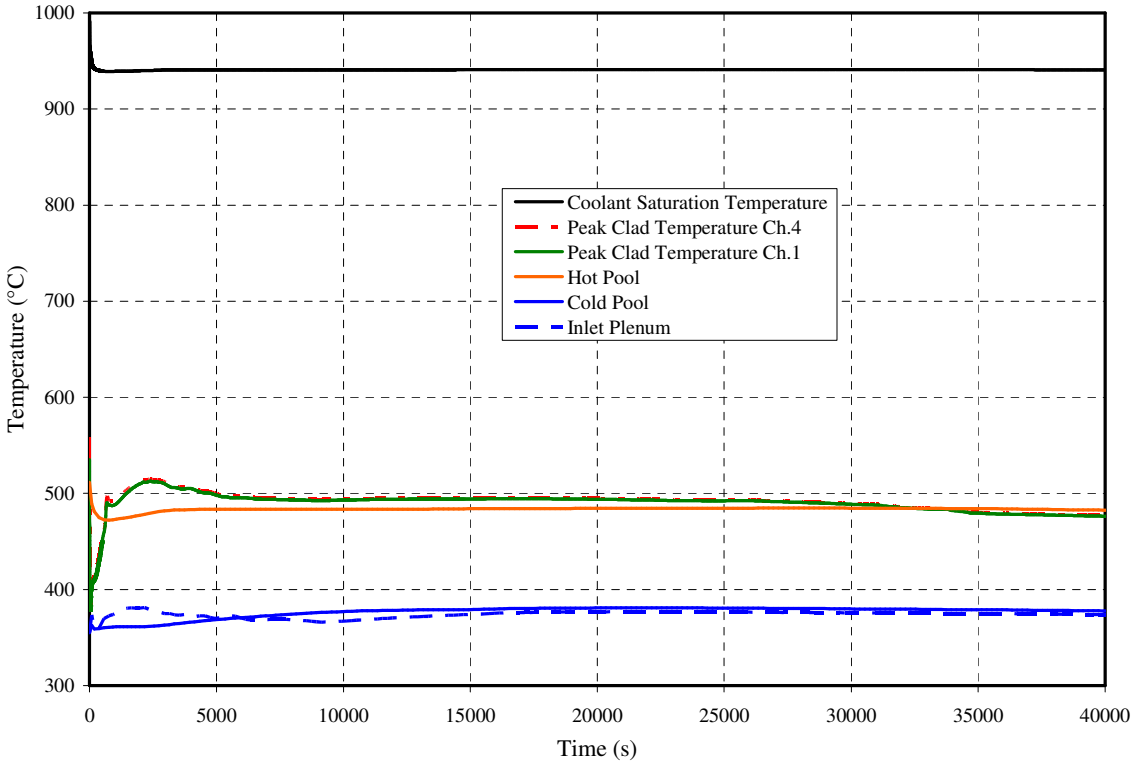

Figure III.7-23: Oxide Fuel PLOF Temperature History, Extended Times

cladding temperatures follow the inlet plenum temperature history to a large part, as the inlet channel flows start to stabilize and a long-term natural convection quasi-equilibrium is reached.

The significance of the PLOF analysis results is emphasized in Figure III.7-22 which shows the initial peak cladding temperature (558°C) in channel 4, compared to the short-term transient peak cladding temperature of 510°C and the long-term peak cladding temperature just above 470°C at around 5 hours before the cool-down begins to take effect. In the PLOF transient, no cladding failures would occur, and the long-term peak temperatures in the accident are lower than the normal operating temperatures. Stated in another way, the long-term temperature safety margins in the accident are greater than the margins at the normal operating conditions. This very significant result is obtained as a result of the natural circulation capabilities of the reactor coolant system and the DRACS.

Unprotected Loss-of-Flow (ULOF) Accident Sequence

a) Base Case

The oxide fuel ULOF transient is initiated by the same set of failures as for the PLOF accident (loss of forced flow and loss of normal heat rejection). However, for the ULOF case, the reactor protection system also fails to scram the reactor; so the accident proceeds from full power. All heat rejection is through the DRACS, with a design heat rejection of 0.5% of full power at nominal conditions. Results from the analysis of the ULOF accident sequence are shown in Figures III.7-24, III.7-25, and III.7-26. Similar to the PLOF accident, there is an early transient period which is driven mostly by the pump coast down. Then, there is a later period when a long-term quasi-equilibrium is being reached, the response is driven more by temperature distributions within the hot and cold pools and the thermal boundary conditions. However unlike the PLOF, in this accident there is coupling between the power history and the thermal response through the passive core reactivity feedbacks since the core is not shutdown through a scram. This two-way coupling is reflected in the results presented below.

Figure III.7-24 shows the histories for the total reactor power, the decay heat production, and the coolant flow in channel 4 (the peak inner core assembly). The power-to-flow imbalance during the first 100 seconds results in significant transient reactor heating. Core outlet fuel, peak clad, and coolant outlet temperatures for channel 4 are shown in Figure III.7-25. Coolant and cladding temperatures increase to approximately 750°C within the first 100 seconds. In contrast, the fuel temperature drops to 1100°C as the coolant heating causes the reactivity feedbacks shown in Figure III.7-26 with the net reactivity dropping to about 15 cents subcritical, which is a considerably smaller feedback than in the metal-fueled case. Control-rod driveline and radial expansion are the main contributors to the initial negative reactivity feedback, which causes power and fuel temperatures to decline. Shortly after the onset of the transient, higher-temperature coolant begins washing over and heating the control-rod drivelines. As the drivelines expand, an additional negative reactivity component is introduced, as shown in Figure III.7-26. Reduced fuel temperatures provide a significant positive Doppler feedback due to the low thermal conductivity and therefore the relatively high initial operating temperatures of oxide fuel. The power-flow ratio reaches a quasi-asymptotic value higher than the initial value of one towards the end of this period, so the channel

coolant and clad temperatures which are initially driven by this, reach a quasi-equilibrium higher than the initial temperatures. The net reactivity has reestablished a quasi-equilibrium around critical, and the fission power remains by far the largest component of the total power. At 400 seconds into the transient, the total power is still above 10% nominal.

The flow coast-down provided by the inertia of the primary pumps ends at approximately 650 seconds when the shafts stop turning. At this point, natural circulation has not yet been fully established, so with the abrupt drop in flow the cladding, and local coolant temperatures begin to rise to form a second temperature peak of about 800°C at approximately 700 seconds. There is less of a rise in the fuel temperature. The increased temperatures provides additional driving force to aid in establishing natural circulation flow and the coolant flow rate in channel 4 begins to increase. But the second temperature peak also causes additional thermal expansion and negative reactivity feedback and this starts a period of oscillations between the fission power and the thermal hydraulic feedback effects. The oscillations are damped oscillations and the conditions eventually reach quasi-equilibrium. At 6000 seconds the fission power is still a large part of the total power and the residual heating is still affected by the fission power. Decay heat now makes a significant contribution but changes in reactivity feedback (particularly the control rod drive line expansion) still have impact on subsequent transient development.

As natural circulation is being established, and with changes in the channel inlet temperatures, the peak in the coolant temperature moves up through the core and to the subassembly outlet. While the delay in observing the temperature peak at the outlet is partly due to the low flow conditions, a bigger contributor to the delay is the large thermal inertia of the structural materials above the core, which must all be heated before the temperature peak reaches the outlet. This affects the hot pool temperature distributions for establishing a quasi-equilibrium natural circulation. Nevertheless, the development of natural circulation holds the peak coolant and cladding temperatures to around 800°C. The peak fuel temperatures follow. Beyond 6000 seconds, the normalized power-to-flow remains quasi-constant and the channel temperatures do not increase significantly. In the long term beyond 20000 seconds, the total power still remains above the heat rejection capability of the DRACS, and overall system temperatures is still slowly rising. The core inlet temperature continues to rise and with it, the channel temperatures. The fission power is still a significant contributor.

The significance of the ULOF accident analysis results is captured in Figure III.7-25. As shown for channel 4, fuel temperatures are well below the melting point. In contrast, the peak cladding and coolant temperatures approach but remain below the coolant saturation (boiling) temperature, with a minimum margin to coolant boiling of about 150°C. This result comes about because of the low thermal conductivity and relatively high operating temperature of oxide fuel. The analysis suggests that parametric variations on the reactivity feedback coefficients, in particular the control rod drive line expansion worth and enhanced scram capability, would be advisable. Results from these parametric variations are presented below.

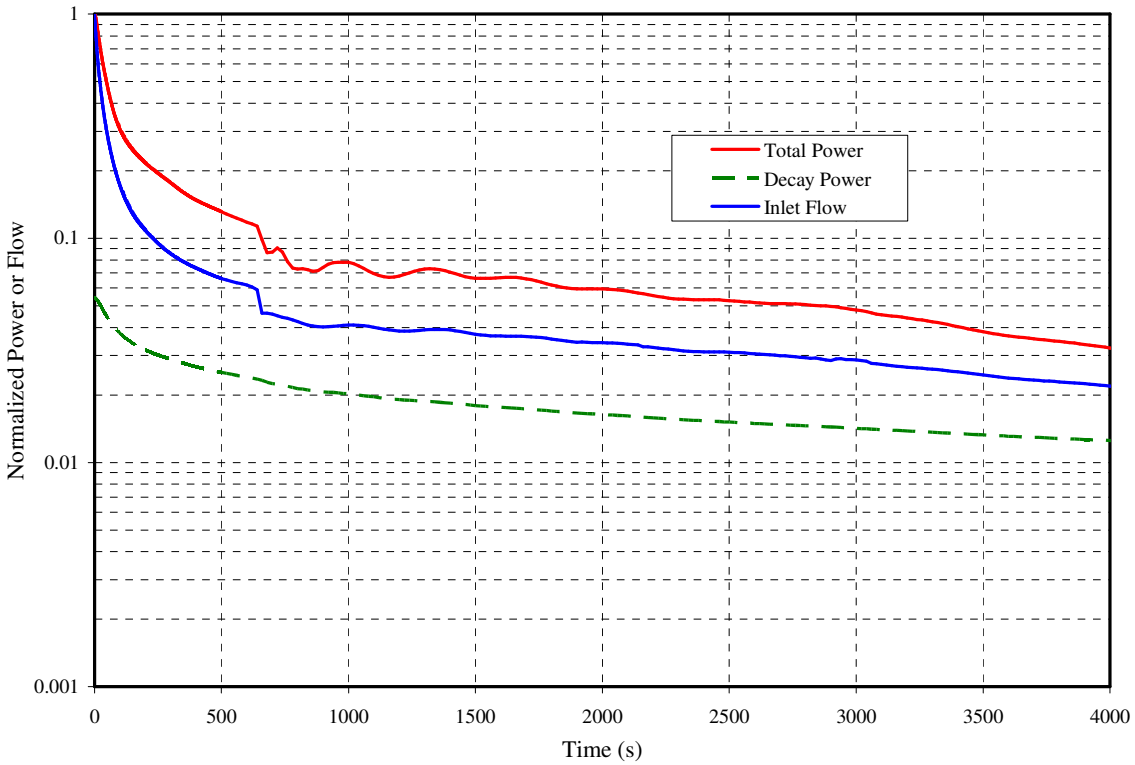

Figure III.7-24: Oxide Fuel ULOF Transient Power and Channel 4 Flow

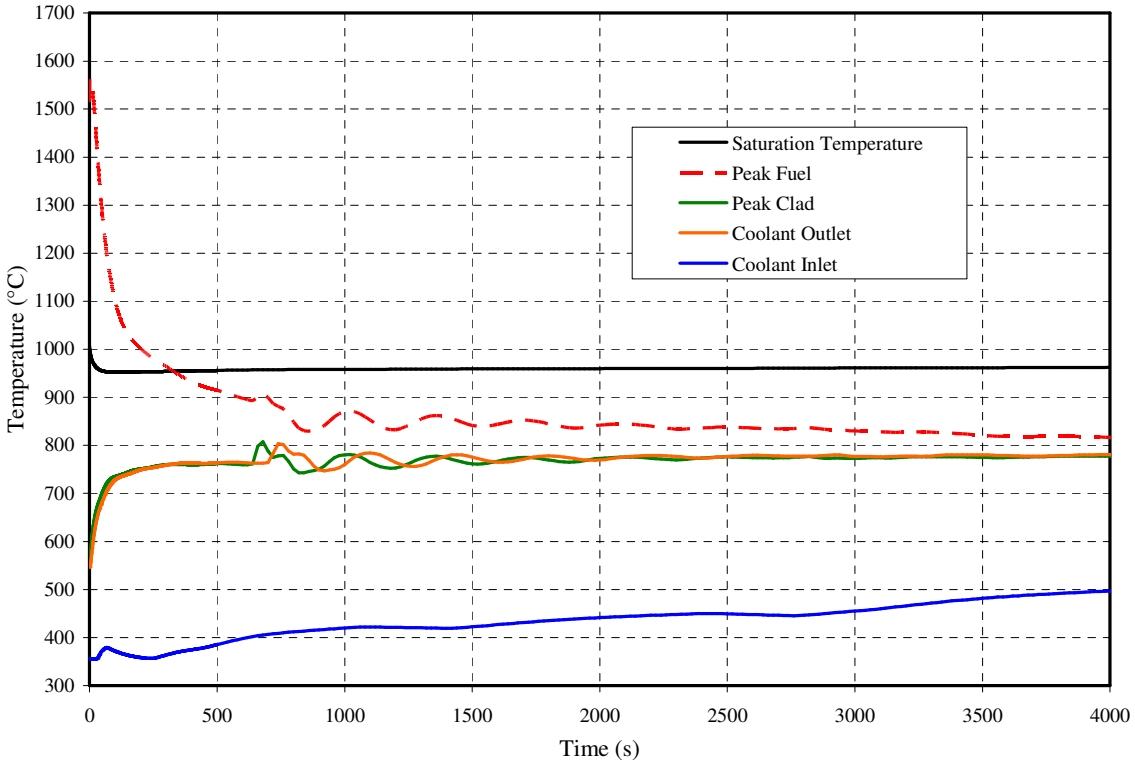

Figure III.7-25: Oxide Fuel ULOF Transient Temperatures for Channel 4

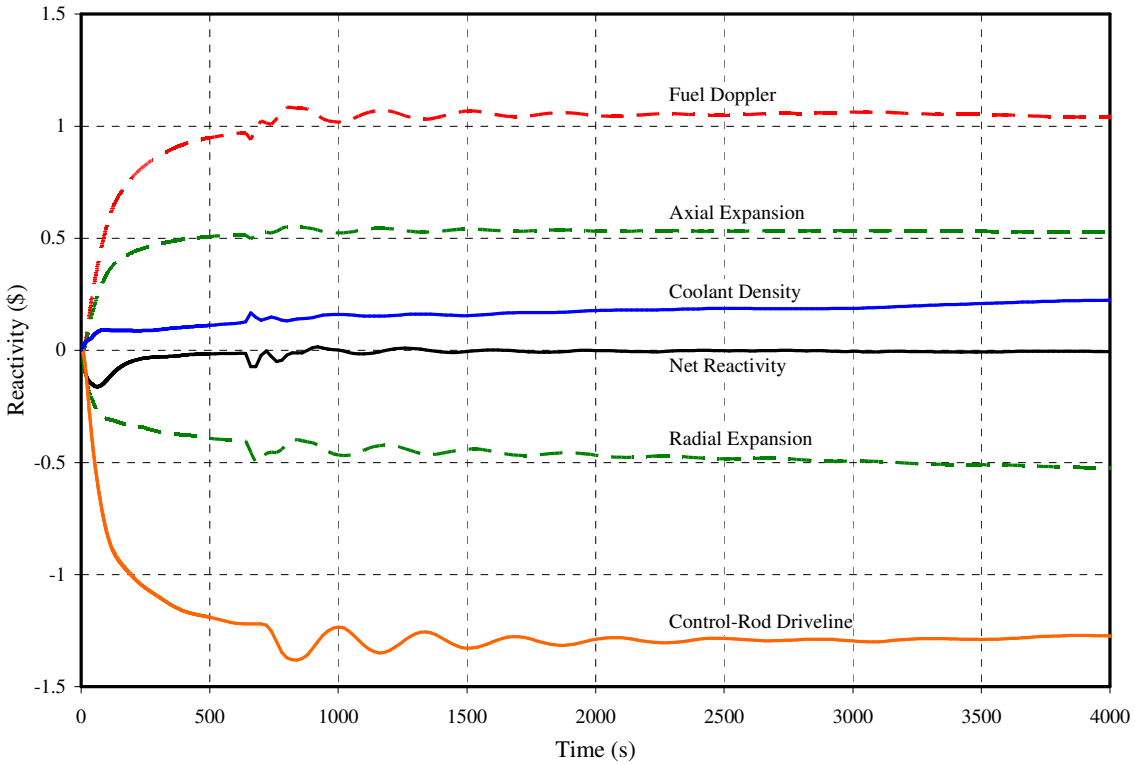

Figure III.7-26: Oxide Fuel ULOF Transient Reactivity Feedback

b) Reduced CRDL Feedback Case

A parametric variation has been performed for the oxide-fueled core with reduced CRDL feedback. Reference should be made to the discussion above for the base case (a). In this parametric case, the worth fitting coefficients for the control rod driveline expansion feedback model have been reduced from the base case by 50%. This is approximately equivalent to reducing the worth by a factor of two and could be viewed as more appropriate for an EOEC case with the rods withdrawn. The ULOF transient is initiated by the same set of failures as for the base case (loss of forced flow and loss of normal heat rejection) and the reactor protection system also fails to scram the reactor; so the accident proceeds from full power. All heat rejection is through the DRACS, with a design heat rejection of 0.5% of full power at nominal conditions. Results from the analysis of this ULOF accident sequence are shown in Figures III.7-27, III.7-28, and III.7-29. The same overall trends can be seen when compared with the base case; however the core temperature margins are significantly reduced.

Figure III.7-27 shows the histories for the total reactor power, the decay heat production, and the coolant flow in channel 4 (the peak inner core assembly). It can be seen that the fission power decreases as the transient proceeds but is noticeably higher than in case (a). Core outlet fuel, peak clad, and coolant outlet temperatures for channel 4 are shown in Figure III.7-28. Coolant and cladding temperatures increase to approximately 850°C within the first 200 seconds. In contrast, the fuel temperature drops to about 1100°C as the heating causes the reactivity feedbacks shown in Figure III.7-29 with the net reactivity dropping to about the same as in case (a). The channel 4

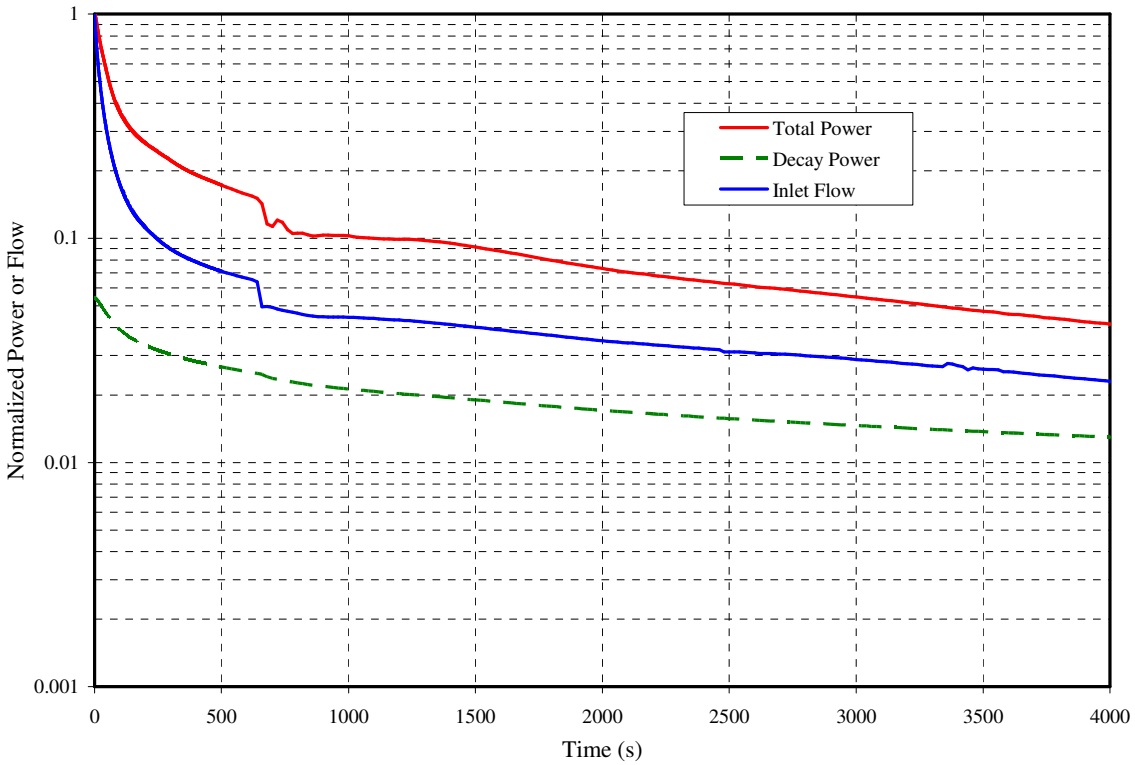

Figure III.7-27: Oxide Fuel ULOF Transient Power and Channel 4 Flow (50% CRDL Feedback)

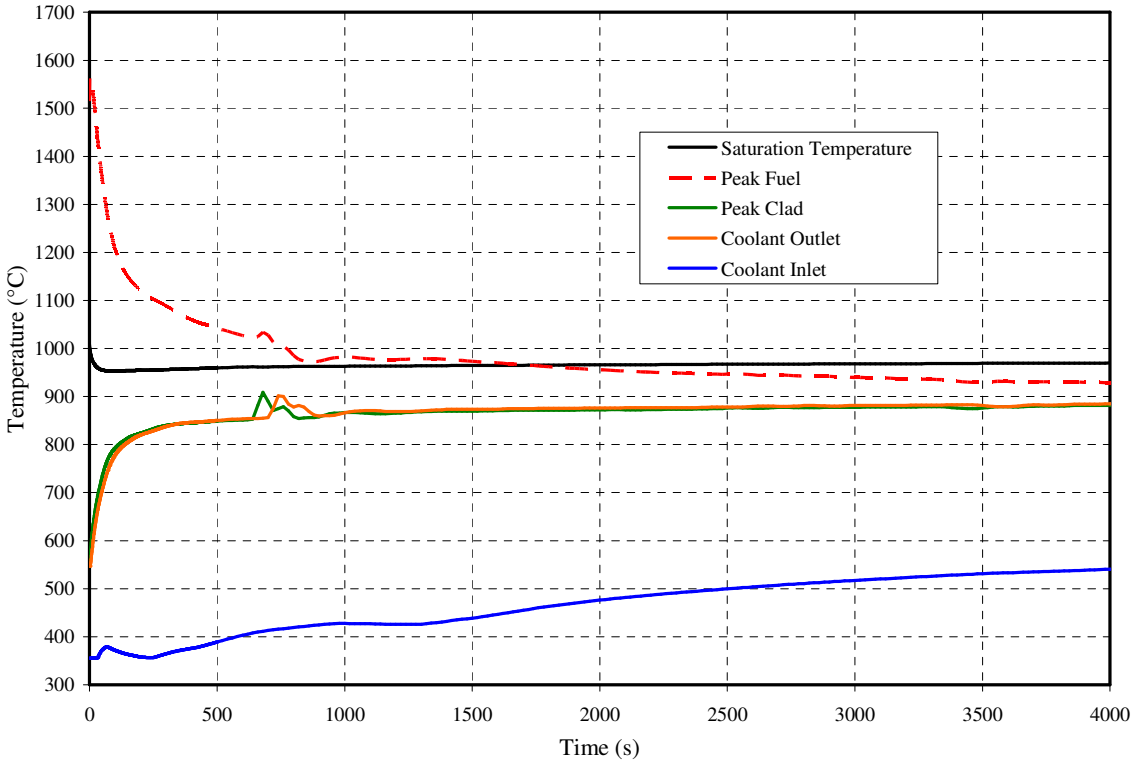

Figure III.7-28: Oxide Fuel ULOF Transient Temperatures for Channel 4 (50% CRDL Feedback)

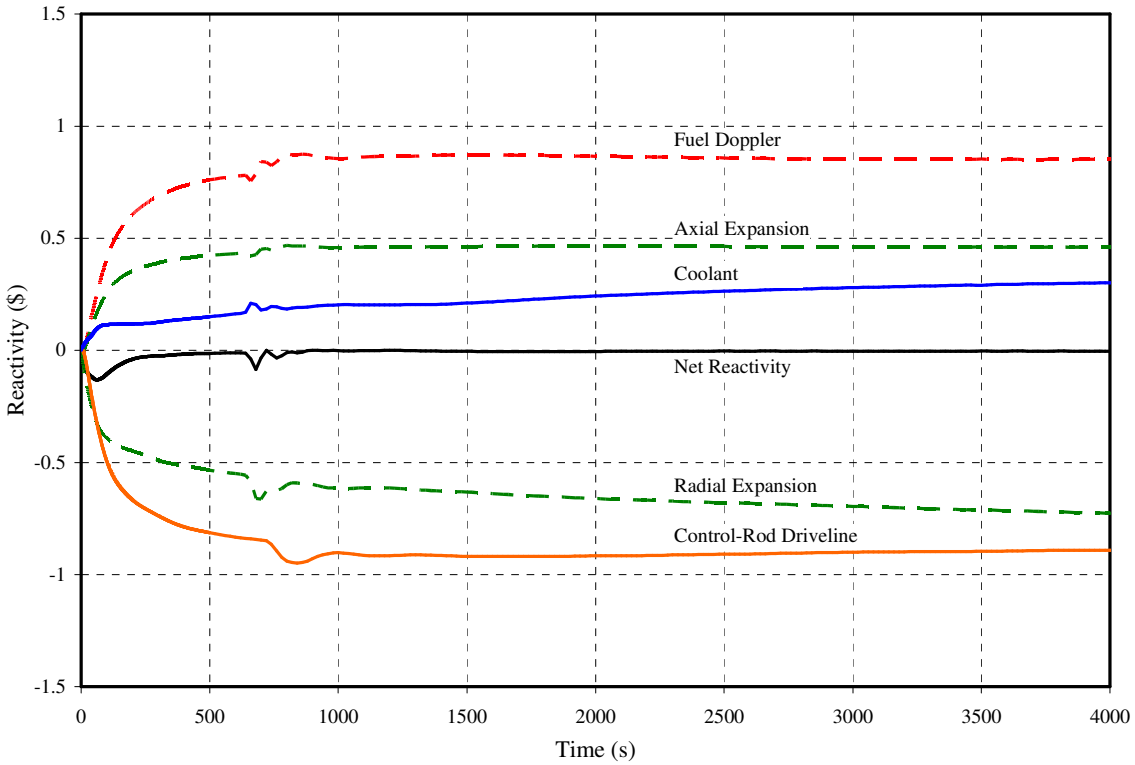

Figure III.7-29: Oxide Fuel ULOF Transient Reactivity Feedback
(50% CRDL Feedback)

temperatures are higher than in case (a). As with case (a), control-rod driveline and radial expansion are the main contributors to the initial negative reactivity feedback but the contribution is reduced by about 30% for the control-rod driveline feed back. The power-flow ratio reaches a quasi-asymptotic value towards the end of this period, so the channel temperatures which are initially driven by this, reach quasi-equilibrium and follow the core inlet temperature. As in the base case, the net reactivity has re-established a quasi-equilibrium around critical but at higher power and higher core temperatures.

As in the base case, the flow coast-down provided by the inertia of the primary pumps ends at approximately 650 seconds when the shafts stop turning. Similarly at this point, natural circulation has not yet been fully established, so with the abrupt drop in flow, the cladding and local coolant temperatures begin to rise to form a second temperature peak around 900°C at approximately 700 seconds. There is less of a rise in the fuel temperature. As in case (a), the second temperature peak also causes additional thermal expansion and negative reactivity feedback and this once again starts a period of damped oscillations between the fission power and the thermal hydraulic feedback effects. But the oscillations are damped out much sooner than in the base case and the conditions soon reach a quasi-equilibrium at about 1000 seconds. Beyond this point the fission power is noticeably a larger part of the total power than in case (a). As in case (a), in the long term beyond 20000 seconds, the total power still remains above the heat rejection capability of the DRACS and overall system temperatures are still rising. At 20,000 seconds, the development of quasi-equilibrium natural circulation conditions continues to hold peak

coolant and cladding temperatures to around 850°C which is about 50°C higher than the base case.

The significance of this ULOF CRDL feedback parametric is best illustrated in Figure III.7-28. As shown for channel 4, fuel temperatures are well below the melting point. In contrast, the peak cladding temperatures approach 900°C. Moreover, the major significance of this ULOF accident parametric analysis is that for channel 4, during the transient, the minimum margin to coolant boiling is now only about 50°C. The analysis further suggests that examination of an enhanced scram shut down capability would be advisable. Results from these parametrics are presented below.

c) SASS Case with Reduced CRDL Feedback

Reference should be made to the discussion above for the base case (a) and the reduced CRDL feedback case (b). Since case (b) led to the results with the minimum margin to coolant boiling in the core, this reduced CRDL feedback case should provide the more challenging case for examining the quantitative benefits of introducing a SASS device. In this parametric case, the total SASS scram worth is $8.70. The insertion is initiated by the coolant outlet temperature of channel 1 (inner driver subassembly) reaching 727°C (1000K). In line with case (b), the control rod driveline feedback has been reduced from the base case by 50%, and additional details are available in the discussion of that case. This ULOF transient is initiated by the same set of failures as for the base case (loss of forced flow and loss of normal heat rejection) and the reactor protection system also fails to scram the reactor; so the accident proceeds from full power. All heat rejection is through the DRACS, with a design heat rejection of 0.5% of full power at nominal conditions. Results from the analysis of this ULOF accident sequence are shown in Figure III.7-30, III.7-31, and III.7-32. As can be expected, the results are a combination of those from the PLOF accident and the ULOF case (b).

Figure III.7-30 shows the histories for the total reactor power, the decay heat production, and the coolant flow in channel 4 (the peak inner core assembly). It can be seen that the fission power decreases as the transient proceeds along the lines of case (b). SASS scram occurs at 80 seconds after initiation of the transient when the total power has been reduced to 40%. Core outlet fuel, peak clad, and coolant outlet temperatures for channel 4 are shown in Figure III.7-31. Coolant and cladding temperatures increase to approximately 760°C and 780°C respectively within the first 80 seconds at which point scram occurs. In contrast, the fuel temperature drops to about 1250°C at the scram point as the heating causes the reactivity feedbacks shown in Figure III.7-32. The net reactivity is at about 12 cents sub-critical at scram. The minimum channel 4 safety margins occur at this point and are higher than those reported in case (b) since the scram occurs at an early time in the heat up transient. The margin to boiling in channel 4 is about 170°C. Post scram in the transient period beyond 80 seconds, the system response is similar to that of the PLOF sequence.

As in the PLOF sequence, the flow coast-down provided by the inertia of the primary pumps ends at approximately 650 seconds when the shafts stop turning. At this point, natural circulation has not yet been fully established, so with the abrupt drop in flow, the cladding and local coolant temperatures begin to rise to form a second broad temperature peak or plateau around 500°C at approximately 700 seconds. Reference should be made

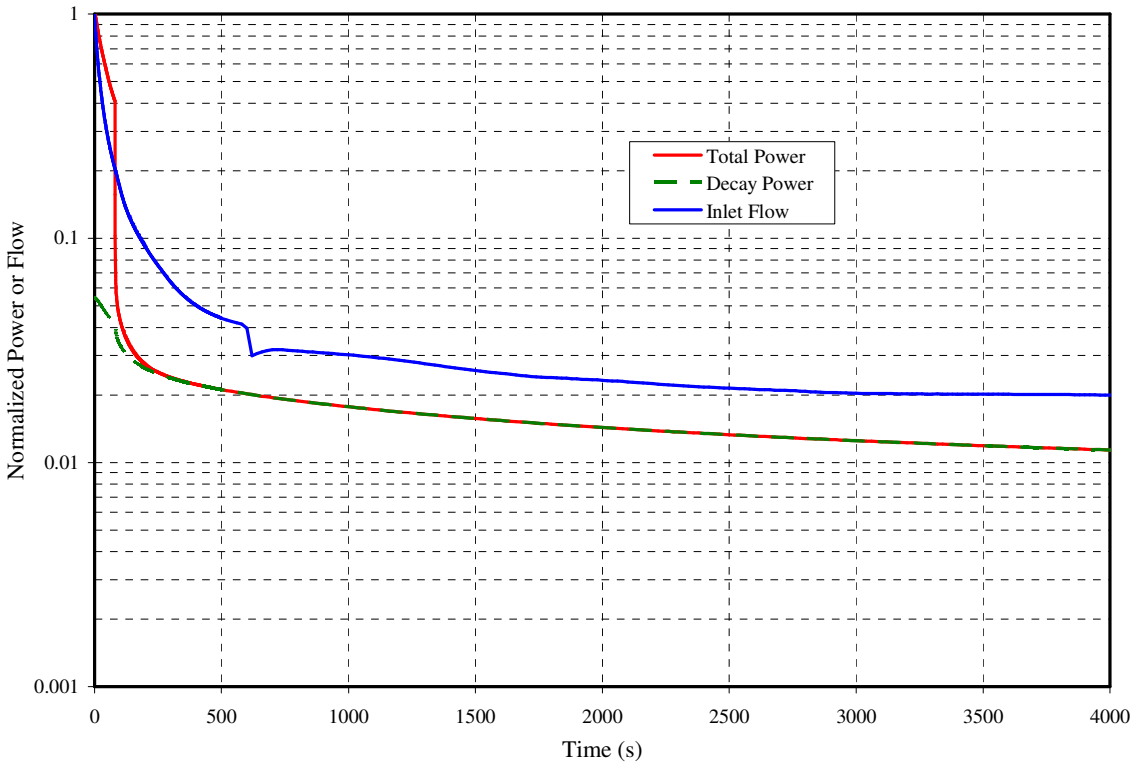

Figure III.7-30: Oxide Fuel ULOF Transient Power and Channel 4 Flow
(50% CRDL Feedback, Secondary Control System Trip at 1000 K)

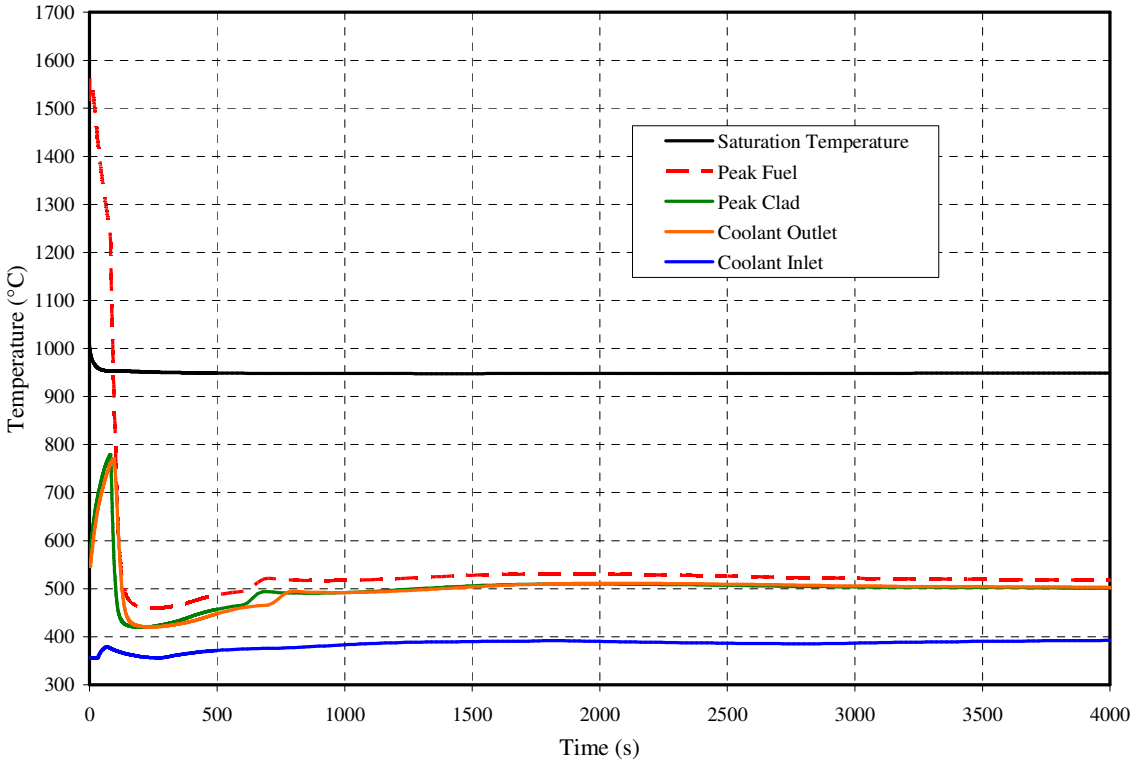

Figure III.7-31: Oxide Fuel ULOF Transient Temperatures for Channel 4
(50% CRDL Feedback, Secondary Control System Trip at 1000 K)

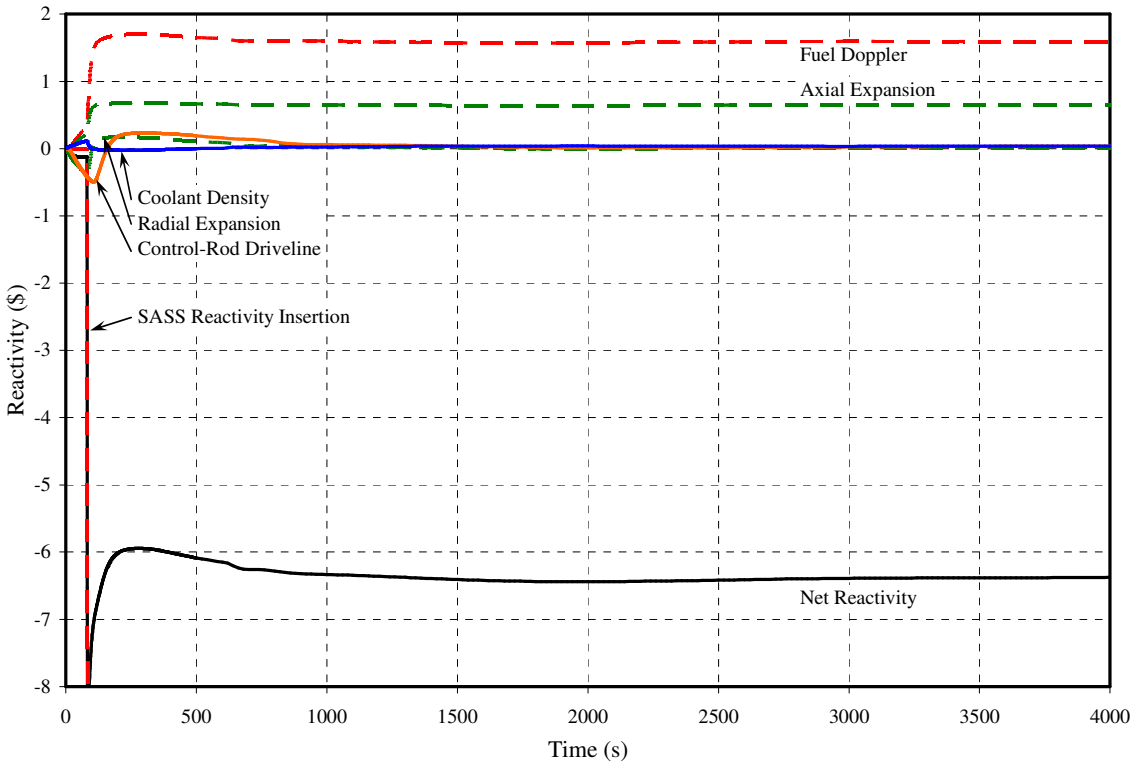

Figure III.7-32: Oxide Fuel ULOF Transient Reactivity Feedback
(50% CRDL Feedback, Secondary Control System Trip at 1000 K)

to the discussion on the PLOF sequence. The transient is now all decay heat driven and the total power eventually decreases to below the heat rejection capability of the DRACS and overall system temperatures decrease. The margins during this phase of the accident are larger than the margins at normal operation.

The significance of the ULOF accident analysis results for the SASS case is confirmed in Figure III.7-31. As shown for channel 4, the inclusion of the SASS has significantly increased the minimum core coolant boiling margin to about 170°C from the 50°C obtained in case (b). Peak cladding temperatures approach 780°C as opposed to 900°C without the SASS in case (b). Fuel temperatures are well below the melting point.

III.7.5 References

1. *American National Standard Decay Heat Power in Light Water Reactors*, ANSI/ANS-5.1-2005, American Nuclear Society, 2005.
2. J. E. Cahalan, A. M. Tentner, and E. E. Morris, "Advanced LMR Safety Analysis Capabilities in the SASSYS-1 and SAS4A Computer Codes," *Proceedings of the International Topical Meeting on Advanced Reactors Safety*, American Nuclear Society, Vol. 2, pp. 1038-1045, Pittsburgh, PA, April 17-21, 1994.
3. L. Leibowitz and R. A. Blomquist, "Thermal Conductivity and Thermal Expansion of Stainless Steels D9 and HT9," *International Journal of Thermophysics*, Vol. 9, No. 5, pp. 873-883, September, 1988.